Variability and Trends of the Amundsen Sea Low since the Early Twentieth Century from Seasonal-Station-Based Reconstructions

RICHARD J. HALL,[a] JULIE M. JONES,[a] RYAN L. FOGT,[b] AND THOMAS J. BRACEGIRDLE[c]

[a] *School of Geography and Planning, University of Sheffield, Sheffield, United Kingdom*
[b] *Department of Geography and Scalia Laboratory for Atmospheric Analysis, Ohio University, Athens, Ohio*
[c] *British Antarctic Survey, Cambridge, United Kingdom*

(Manuscript received 31 March 2025, in final form 15 August 2025, accepted 6 September 2025)

ABSTRACT: The Amundsen Sea is dominated by a quasi-stationary low-pressure region, the Amundsen Sea low (ASL). ASL variability impacts regional weather and the basal melting of ice shelves, an important contributor to sea level rise. To understand trends and variability of the ASL, it is important to have data for a long time period. However, the shortness of the satellite record starting in 1979 and the sparseness of Antarctic observational data prior to this make understanding variability on decadal scales challenging. Century-long reanalyses are available but have well-known pressure biases, meaning that trends cannot be reliably quantified. Other reconstructions are available at the annual resolution but mask important seasonal differences. Here, we reconstruct the ASL at seasonal resolution from 1905, using Southern Hemisphere weather station sea level pressure data, which takes advantage of well-known teleconnections between the tropics and Antarctica, although the strength of these is seasonally dependent and varies decadally. We compare our reconstructions with two centennial reanalyses and ERA5. Our reconstruction captures early twentieth-century variability associated with ice shelf melting and retreat and places recent ASL trends in a longer-term context. We find that the recent deepening of the ASL across all seasons is unprecedented since 1905, and there is increased uncertainty in the ASL index during the mid-twentieth century. We also assess the stationarity of the association between station data and the ASL by using data from a Pacific pacemaker climate model experiment. The stationarity assumption for our ASL reconstruction is valid, except for the austral autumn due to insufficient data availability.

SIGNIFICANCE STATEMENT: Our study provides a novel century-length seasonal reconstruction of pressure in the Amundsen Sea region [the Amundsen Sea low (ASL)]. On interannual time scales, a more positive (weaker) ASL can drive warm water intrusions under the ice shelves, leading to increased melt and significant contributions to sea level rise. The ASL also impacts sea ice and Antarctic temperatures. Reliable records, which start in 1979 in this data-poor region, are not long enough to separate the large natural variability, particularly at decadal scales, from human-induced changes. Our reconstruction compares favorably with those from centennial-scale reanalyses and is free from the high-pressure biases associated with these products. Our new record shows that the recent negative trend in the ASL is unprecedented since the early twentieth century.

KEYWORDS: Antarctica; Atmospheric circulation; Teleconnections; Climate variability; Statistics; Decadal variability

1. Introduction

The Amundsen Sea low (ASL) is a quasi-stationary region of climatological low pressure in the South Pacific sector of the Southern Ocean. It is the deepest of three climatological low pressure centers that exist due to the interaction of the orography of the Antarctic Peninsula with the mean westerly circumpolar winds (Baines and Fraedrich 1989; Goyal et al. 2021) and has the highest sea level pressure (SLP) variability in the world (Fig. 1) (Connolley 1997). It occurs because of the large number of depressions, which either form in the circumpolar trough or move south from midlatitudes (Fogt et al. 2012).

The ASL is linked to both the Southern Annular Mode (SAM; Turner et al. 2013) and variability in tropical Pacific sea surface temperatures (SSTs) via teleconnections such as the Pacific–South American (PSA) pattern (Kidson 1999; Mo and Higgins 1998; Ding et al. 2011). In general, positive El Niño–Southern Oscillation (ENSO) events are related to a weakened ASL (Li et al. 2021); La Niña events typically strengthen the ASL. The strongest correlations between ENSO and the ASL occur in austral spring, when the Rossby waves associated with ENSO variability are at their most energetic (Jin and Kirtman 2009). Phase shifts in other teleconnections that operate on decadal time scales, such as the interdecadal Pacific oscillation (IPO; Henley et al. 2015), have also been found to influence the ASL, in particular a deepening of the ASL over the 1990–2015 period (Meehl et al. 2016; Li et al. 2021).

In addition to internal climate variability, anthropogenic forcing has played a role in historical ASL trends. The deepening in

Denotes content that is immediately available upon publication as open access.

Supplemental information related to this paper is available at the Journals Online website: https://doi.org/10.1175/JCLI-D-25-0159.s1.

Corresponding author: Richard J. Hall, richard.j.hall@sheffield.ac.uk

DOI: 10.1175/JCLI-D-25-0159.1

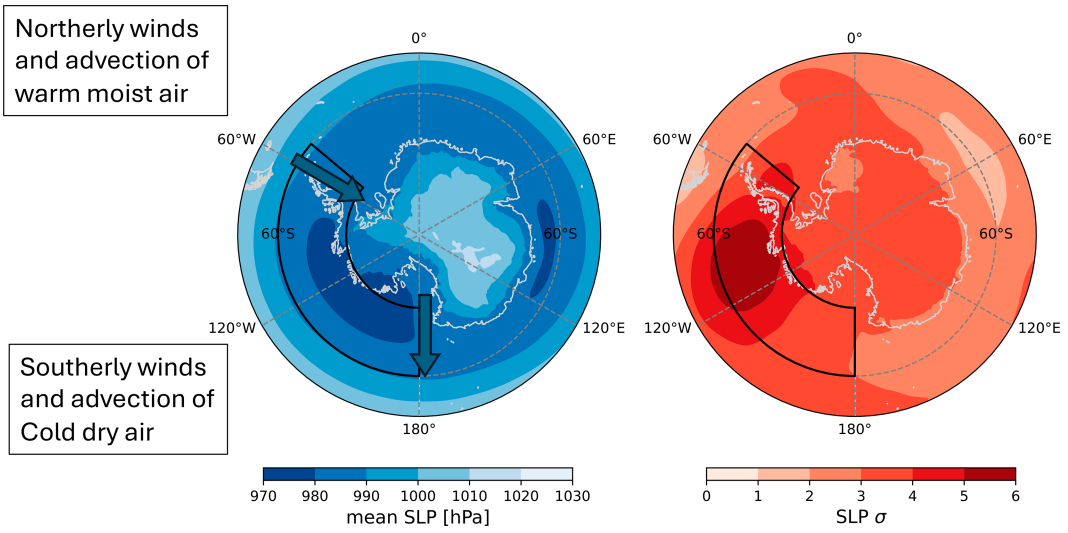

FIG. 1. (a) Mean and (b) SD of SON SLP over the Southern Hemisphere mid–high latitudes, 1979–2023, using ERA5 data. The box shows the region used to calculate the area-averaged ASL index (180°–310°E, 60°–75°S).

recent decades is consistent with model-simulated responses to greenhouse gas increases (Raphael et al. 2016) and, in the austral summer, stratospheric ozone depletion (England et al. 2016; Fogt and Zbacnik 2014). It is, however, difficult to clearly separate anthropogenic forcing from the abovementioned decadal Pacific variability (e.g., Schneider and Deser 2018; Meehl et al. 2016; Fogt and Wovrosh 2015). In light of these various forcing factors, understanding the longer-term history of the ASL is key to better understanding the relative roles of forced and natural variability through the entire twentieth century.

The ASL exerts a strong influence on the climate of West Antarctica and the Antarctic Peninsula (Hosking et al. 2013; Raphael et al. 2016). Cyclonic flow around the ASL advects warm, moist air southward along its eastern flank, and cold, dry air northward along its western flank, together with associated movement of sea ice (Fig. 1). Hence, changes to its strength and location both through time and seasonally (Clem and Fogt 2013) influence the climate of this region.

Understanding the longer-term behavior of the ASL is also important due to the influence of the ASL on the supply of warm Circumpolar Deep Water (CDW) to the West Antarctic continental shelf. The Amundsen Sea region of Antarctica is a significant contributor to sea level rise (Naughten et al. 2023). Ice shelves extend out over the ocean from the Antarctic ice sheet and are melted from below by the intrusion of warm CDW (e.g., Pritchard et al. 2012; Jenkins et al. 2016). This water intrusion varies on multiple time scales driven by oceanic variability, which, in turn, is modulated by the regional winds and the ASL: A weakened (strengthened) ASL increases (decreases) the onshore flow of CDW, which increases (decreases) basal melting of the ice sheet on interannual time scales (Steig et al. 2012; Paolo et al. 2018; Dotto et al. 2020), although Silvano et al. (2022) suggest that on decadal scales, baroclinic influences from the surface wind on the shelfbreak undercurrent may actually have the opposite effect. The oceanic response is nonlinear and is also influenced by bathymetry, mesoscale eddies, and ocean stratification (Turner et al. 2017).

The melting of these ice shelves contributes to ice loss from the West Antarctic Ice Sheet (WAIS) (Dalaiden et al. 2024), resulting in a sea level rise of approximately 4.5 cm (100 yr)$^{-1}$ (Shepherd et al. 2018), the largest contribution of any region in Antarctica (Naughten et al. 2023). Recent studies focus on the hypothesis that ice sheet change in the Amundsen Sea sector is an accumulating response to a series of oceanic warm episodes (e.g., in the 1940s and 1990s) when rapid ice sheet loss was initiated (Jenkins et al. 2018; Holland et al. 2019, 2022). Holland et al. (2022) suggest these episodes are caused by anticyclonic wind anomalies in the Amundsen Sea during these decades. A deeper understanding of this mechanism requires a longer perspective on the ASL, as decadal wind variability is poorly sampled in the relatively short records from reanalysis products, which are only reliably constrained by remote sensing data in the post-1979 modern satellite era (Schneider and Fogt 2018).

The strength of the ASL can be measured by an index, calculated as regionally averaged SLP or geopotential height (e.g., Turner et al. 2013; O'Connor et al. 2021; Dalaiden et al. 2021) or as indices of its relative depth and location (Hosking et al. 2013). These indices can be calculated from reanalysis datasets for the modern satellite era (post-1979) with good reliability due to the enhanced number of observations incorporated within the reanalysis (Bracegirdle et al. 2013). Prior to this, however, observations are much sparser, so there is increased reliance on the reanalysis model to reconstruct atmospheric fields, resulting in greater uncertainty. Reanalyses such as the Twentieth Century Reanalysis (20CR; Compo et al. 2011; Slivinski et al. 2019) allow for a reconstruction of the ASL at seasonal resolution over the whole of the twentieth century, which would in theory allow decadal wind variability to be assessed. However, positive SLP biases south of 60°S in the early twentieth century result in potentially spurious negative SLP

trends over the whole century. Schneider and Fogt (2018) attribute this to large uncertainty and a lack of assimilated data before 1950. Another possibility is a pressure bias due to such reanalysis products failing to conserve atmospheric mass in the early twentieth century prior to the assimilation of satellite data (Trenberth and Smith 2005; Clark and Fogt 2019). A new reanalysis product, the Modern Era Reanalysis (ModE-RA; Valler et al. 2024), combines proxy, documentary, and instrumental data from 1421 to 2008 at monthly resolution and can be used to produce a seasonal ASL index.

The ASL index has been reconstructed at the annual resolution (O'Connor et al. 2021; Dalaiden et al. 2021) to cover the twentieth century and earlier, using data assimilation of proxy records from corals, tree rings, and ice cores into a spatial field constrained by a climate model prior. However, a seasonal resolution is desirable as the ice sheet melting is seasonally variable and the tropical teleconnections show seasonal variations in strength (Scott Yiu and Maycock 2019; Li et al. 2021).

In this study, we present a new reconstruction of the ASL at seasonal resolution based on in situ observations primarily at Southern Hemisphere midlatitudes. Teleconnections between low- and high-latitude climates allow us to use Southern Hemisphere station data outside of the Antarctic with data extending to the early twentieth century. We also present a comparison of our reconstructions with the aforementioned reanalyses, to compare trends and to identify any robust features in ASL behavior since the early twentieth century. These reconstructions will enable a better understanding of the interplay of anthropogenic trends and decadal variability to better constrain projected future sea level rise than is currently available from satellite-era reanalyses.

2. Data and methods

a. *The ASL index from reanalysis*

We calculate the predictand ASL indices for model fitting using monthly mean ERA5 SLP at 0.25° horizontal grid spacing (Hersbach et al. 2020) for 1979–2023. We also extend the indices back to 1940 for comparison with our reconstructions.

For comparisons in the early part of the twentieth century, we calculate the ASL index from the most recent version 3 of the 20CR (20CRv3; Compo et al. 2011; Slivinski et al. 2019). We also use the ensemble mean of ModE-RA (Valler et al. 2024), which provides monthly mean fields of SLP anomalies at approximately 1.8° horizontal resolution. An offline data assimilation approach is used, with a 20-member ensemble of the ECHAM6 model. Full details are in Valler et al. (2024). As the ModE-RA data are stored as anomalies with respect to 1901–2000, we calculate normalized anomalies relative to 1979–2008, to match as closely as possible our reconstructed ASL.

We calculate the ASL index as the standardized spatial mean SLP area weighted over 60°–75°S, 180°–310°E (O'Connor et al. 2021; Turner et al. 2013). We also explore the potential for reconstructing the location and relative depth of the ASL, described by Hosking et al. (2013), which summarize its location and strength. The actual central pressure (ACP) is the minimum SLP occurring within the ASL region, and sector pressure (SP) is the mean SLP calculated over the region (similar to the O'Connor ASL index outlined above). The relative central pressure (RCP) is then the difference between the actual SLP field and the sector-mean pressure. The longitude and latitude of the ASL are significant as the location of the low will influence the direction of winds over the Amundsen Sea region and associated atmospheric and oceanic conditions. The longitude and latitude are calculated as the location of the RCP.

To reliably reconstruct the ASL from in situ weather station observations prior to the late 1950s, when regular station observations were established at several locations across the Antarctic continent, available SLP station observations at lower latitudes can be used at locations where SLP variability is significantly related to ASL variability. Figure 2 shows ERA5-derived maps of time series correlations between some of the abovementioned indices and SLP at all grid points over the Southern Hemisphere. We apply the false discovery rate (FDR; Benjamini and Hochberg 1995; Wilks 2016) when considering multiple correlations and regressions over a field to guard against multiple testing resulting in spuriously labeling correlations as statistically significant.

ACP and SP are not shown as these indices correlate closely with the area-averaged ASL index of O'Connor et al. (2021) and hence have similar correlation patterns with the Southern Hemisphere SLP field and are not used further in this study. The area-averaged ASL index shows the greatest reconstruction potential, with the largest regions of significant correlations over midlatitude land areas. It is evident that RCP is a local phenomenon (Fig. 2), representing the strength of the regional pressure gradient in the South Pacific Ocean, and cannot be reliably reconstructed from station data, as areas of significance are very small and mostly lie within regions where there are no instrumental observations. In addition, there are weaker but quite widespread correlations between the ASL latitude and longitude and hemispheric SLP, so we also reconstruct these indices.

b. *The predictor data*

The predictors in the reconstructions are monthly mean station SLP observations from the list of weather stations shown in Table 1. These are stations that have been used in other reconstructions of Antarctic climate over the twentieth century, including the SAM (Jones et al. 2009), Antarctic pressure (Fogt et al. 2016a,b), and Antarctic sea ice (Fogt et al. 2022). Collectively, they represent the largest network of nearly continuous SLP observations across the Southern Hemisphere extending back to the late nineteenth century. Several patching and quality control approaches have been used to enhance the temporal continuity of the network, some of which are described below. To supplement the observations from midlatitudes, observations from Antarctic stations with the most continuous/complete records are retrieved from the Reference Antarctic Data for Environmental Research (READER) dataset (Turner et al. 2004). The quality-controlled midlatitude data are derived from the University Corporation for Atmospheric Research (UCAR) dataset "World Monthly Surface Station Climatology" d570000. There are gaps in some of these series. We patch some of these

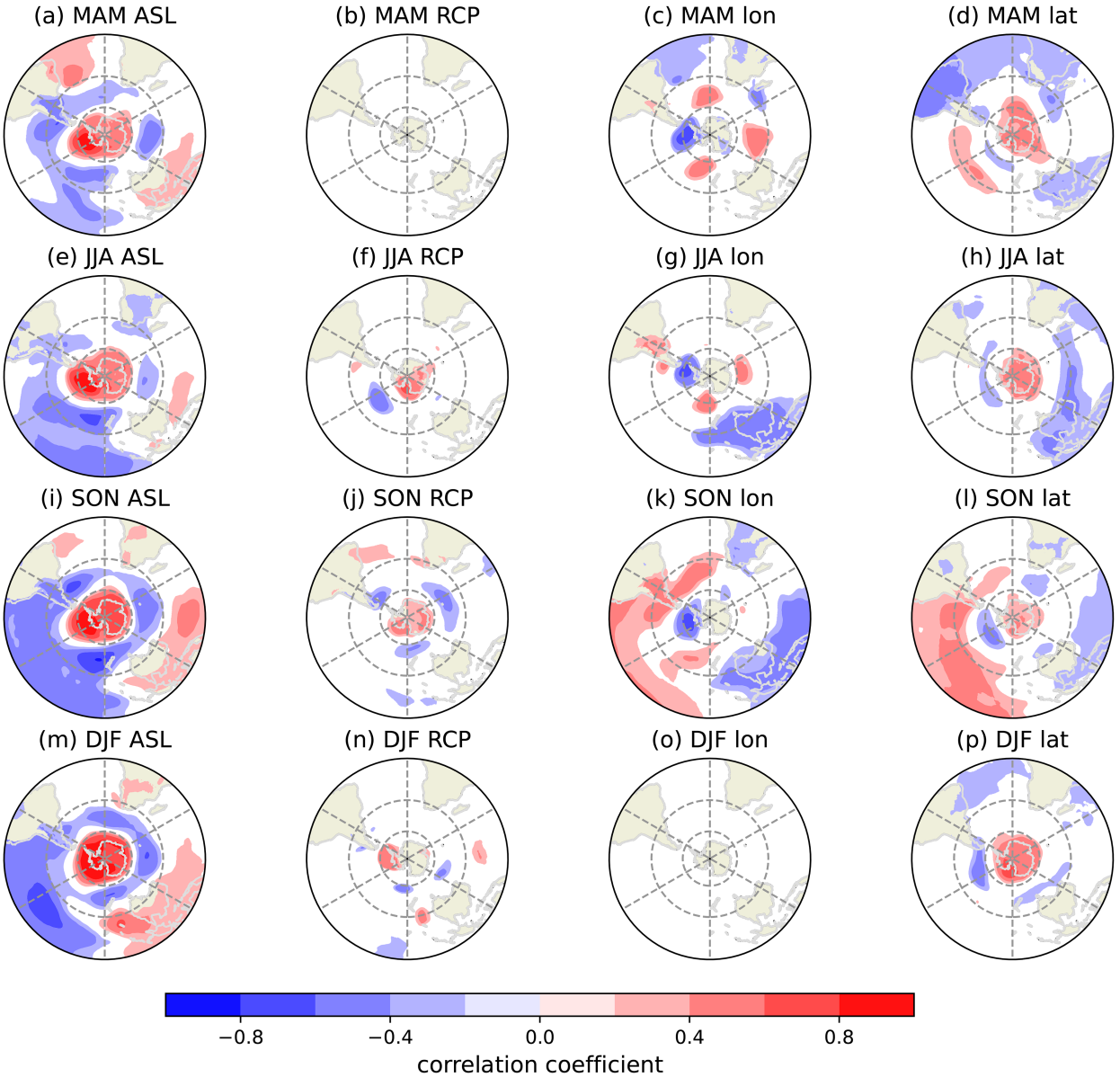

FIG. 2. Correlations of the detrended ASL indices for all seasons with the detrended Southern Hemisphere SLP standardized anomalies, 1979–2023. Only significant ($p < 0.1$) correlations are shown. The FDR is applied to the significance fields.

using station data from the KNMI Climate Explorer and the monthly mean observations used in the construction of the HadSLP2 SLP dataset (Allan and Ansell 2006). We only implemented this patching if time series values for the months before and after the missing values closely resembled those of the data used in previous reconstructions (Fogt et al. 2016a,b) in terms of magnitude and direction of change from month to month. For data points that we could not patch from these sources, we also obtain WMO station data at hourly, daily, or monthly resolutions using the Python "Meteostat" package, which allows direct access to these data. Additionally, we use data from the International Surface Pressure Databank v4 (Compo et al. 2019). Here, data for individual stations can be obtained at subdaily resolution. For both these datasets, we remove any extreme outliers [±5 standard deviations (SDs) from the mean] from the daily or subdaily data before calculating monthly means, which are only calculated if more than 50% of days in the month have a daily mean value. Again, patching only occurs if time series values from these datasets before and after any missing months closely resemble the data from ds570000. Seasonal means are calculated from the monthly mean station data after patching, weighting the calculation by the length of each month, and are only calculated if 2 of the 3 months in the season have an observed value at that station. There are a few months missing after patching. For stations with data available since 1941, 32 out of 37 stations had 10 or fewer missing

TABLE 1. Stations used in the analysis. Only stations which show a significant correlation ($p < 0.1$) with at least one ASL index are shown. The symbol # denotes stations only significant at $p < 0.1$, and others are significant at $p < 0.05$; blank values show that there is no significant correlation. Square brackets denote a significant correlation but with gaps in the 1979–2023 time series. Other stations considered which have no significant correlations are Saint Helena, Rio de Janeiro, and Santiago.

Station	Availability	MAM	JJA	SON	DJF
New Amsterdam Island	1951–2023	−0.47	−0.26#	−0.49	−0.44
Kerguelen Island	1953–2023			−0.57	−0.34
Durban	1912–2023		−0.29#		
Cape Town	1900–2023		−0.27#		[0.32]
Port Elizabeth	1900–2023		−0.31		
Gough Island	1956–2023			−0.36	−0.52
Marion Island	1948–2023				−0.38
Antofagasta	1951–2023			−0.36	−0.26#
La Serena	1941–2023		[−0.29]#	[−0.52]	−0.53
Juan Fernandez Island	1911–2023	−0.47	−0.33	−0.28#	−0.32
Valdivia	1900–2023	−0.49	−0.3#	−0.49	
Punta Arenas	1900–2023		0.35		
Salta	1901–2023	[−0.48]	−0.27#	[−0.39]	
Resistencia	1951–2023	−0.39	−0.26#	−0.38	
Catamarca	1901–2023	−0.55		−0.59	−0.35
Cordoba	1900–2023	[−0.54]	−0.35	−0.49	[−0.3]
Rosario	1951–2023	−0.46	−0.34	−0.38	
Pehuajó	1951–2023	−0.46	−0.39	−0.43	
Junin	1951–2023	−0.54	−0.3#	−0.42	−0.28#
Ezeiza	1951–2023	−0.54	−0.28#	−0.32	
Buenos Aires	1900–2023	−0.47	−0.34	−0.36	
Santa Rosa	1951–2023	−0.38		−0.49	−0.26#
Mar del Plata	1941–2023	−0.37		−0.4	−0.4
Neuquén	1957–2023	[−0.41]		−0.34	−0.29#
Bahía Blanca	1939–2023	−0.38	−0.26#	−0.36	−0.38
Trelew	1941–2023	−0.29#		−0.53	−0.31
Sarmiento	1903–2023	−0.27#		−0.43	−0.32
Comodoro Rivadavia	1951–2023	−0.27#		−0.37	−0.34
Orcadas	1903–2023				0.4
Koumac	1951–2023				0.62
Nouméa	1941–2023				0.64
Nandi	1947–2023	−0.29#	−0.29#		
Tahiti	1900–2023	−0.34	−0.38	−0.38	−0.55
Auckland	1900–2023	−0.32	−0.33	−0.51	
Wellington	1900–2023	−0.32	−0.49	−0.66	−0.42
Hokitika	1900–2023	−0.26#	−0.4	−0.59	
Christchurch	1901–2023	−0.31	−0.47	−0.63	−0.46
Dunedin	1918–2023	−0.32	−0.51	−0.62	−0.5
Campbell Island	1941–2023	[−0.34]	[−0.45]	−0.56	[−0.67]
Chatham Island	1900–2023	−0.41	−0.57	−0.78	−0.52
Carnarvon	1951–2023	0.3			0.32
Port Hedland	1951–2023	0.28#	0.25#		
Alice Springs	1900–2023				
Meekathera	1951–2023				0.28#
Charleville	1951–2023				0.31
Brisbane	1900–2023				0.28#
Perth	1900–2023				0.27#
Kalgoorlie	1941–2023				
Ceduna	1951–2023				
Adelaide	1900–2023				
Sydney	1900–2023				
Melbourne	1903–2023				
Hobart	1900–2023			−0.34	−0.27#
Norfolk Island	1951–2023				0.49
Macquarie	1950–2023			−0.52	−0.52
Isla de Pascua	1948–2023	−0.27#	−0.42	−0.38	−0.46
Total [including incomplete stations]		27[31]	26[28]	32[34]	33[36]

months out of a total of 997 months. Any missing month was found to have little effect on the seasonal time series in tests where a month from each season (the worst-case scenario) was removed at random and seasonal means calculated from 2 instead of 3 months. Correlations with the seasonal means calculated from the full monthly time series were very high (e.g., 0.85 for Campbell Island in the midlatitudes and 0.95 for Tahiti in the tropics).

c. *Reconstruction using principal component regression*

We use principal component regression (PCR) to reconstruct the ASL index, whereby multiple ordinary least squares linear regression is applied to estimate the ASL index from the leading PCs of station observations. PCR was first used for climate reconstruction from tree rings (Briffa et al. 1986; Cook et al. 1999) and has been successfully employed in climate index reconstruction (Jones and Widmann 2003, 2004; Jones et al. 2009; Hannaford et al. 2015; Barrett et al. 2018a,b; Fogt et al. 2022).

The fitting period for the data is 1979–2023. We linearly detrend and standardize the station data and the ERA5 ASL index over this period and correlate each station time series with the ASL index for the relevant season over the period 1979–2023. For each season, we retain a subgroup of those stations with a significant correlation. To create the predictor PCs, we conduct an empirical orthogonal function (EOF) analysis on the time series of each subgroup of significant stations for each season, initially obtaining the first 10 EOFs. We then retain those PCs as predictors which have a significant correlation with the ASL index, using the same significance level as that between the ASL index and the individual stations used in station selection. To create a miniensemble of reconstructions, we retain different groups of stations based on different significance thresholds ($p < 0.1$ and $p < 0.05$) and use each to create a slightly different version of the reconstruction. Furthermore, for each of the significance thresholds, we create reconstructions of different lengths, according to station availability. These reconstructions extend from 1905 to 2023, 1941 to 2023, and 1957 to 2023, making use of additional observations becoming available toward the present. We also investigate whether the inclusion of Antarctic observations leads to a large improvement in reconstructions. Antarctic station data are only available consistently for the 1957–2023 period (Turner et al. 2004), and we make these Antarctic plus (ANT+) reconstructions for each of the significance thresholds above.

We perform multiple ordinary least squares linear regression using the selected PCs as predictors of the ASL index. To ensure that this model is not overfitted, we use leave-one-out cross validation to produce a cross-validated model fit, due to the short length of the fitting period. In Fogt et al. (2016a,b), two different 30-yr calibrations and separate validation periods were used. Those reconstructions with shorter validation periods obtained similar reconstructions in each case, so we maximize the calibration period to capture the most observed variability in our model. To avoid autocorrelation of the time series, we additionally omit the two data points on either side of the validation year. Measures of fit include the Pearson correlation coefficient, the coefficient of multiple determination R^2, root-mean-square error (RMSE), and the mean absolute error (MAE). All time series of the ASL, and principal components, are standardized relative to the fitting period (1979–2023).

To calculate the PCs used to obtain the reconstructions over the whole time period, we project the station anomalies for each subgroup of significant stations onto the EOFs calculated over the fitting period and then standardize them by the mean and standard deviation of the fitting period. The regression coefficients obtained during model fitting are then applied to these PCs to obtain the final reconstructions.

As an alternative method of PC selection, we used the Bayesian information criterion (BIC) to determine which PCs should be retained for the regression model. This approach was generally more liberal than our method above and resulted in a greater number of PCs being incorporated into the multiple regressions. Overall, this approach made little difference to the measures of fit. While there were some frequent slight improvements in the models, for the ANT+ reconstructions in particular, the models were clearly overfitted (using seven PCs) and performed poorly in out-of-sample comparisons. Our method of PC selection is therefore more conservative but does not produce the overfitting experienced with some of the BIC models. Statistical values for the BIC models are included in Table S1 in the online supplemental material.

d. *Stationarity assumptions*

The fidelity of the reconstruction depends on the statistical relationship between station SLP observations and the ASL remaining stable through time. As testing this is not possible with observational data over multidecadal time scales, to examine the potential stationarity over time of the statistical associations between station time series and the ASL index, we use the Pacific pacemaker simulations of the Community Earth System Model, version 2 (CESM2; Danabasoglu et al. 2020), as a pseudoreality. In this simulation, which contains 10 ensemble members, at 1° horizontal resolution, eastern tropical Pacific SST anomalies are timeevolving but nudged toward observations [National Oceanic and Atmospheric Administration Extended Reconstructed SST, version 5 (NOAA ERSST 5; Huang et al. 2017)]. This ensures that the observed ENSO evolution is retained in each member. The nudging is full strength between 15°S and 15°N and from the date line to the American coast with a 5° latitude buffer region to the north and south where the strength of the nudging is reduced in a linear fashion. West of the date line, the nudging mask is a wedge shape tapering toward the Maritime Continent. We obtain monthly mean SLP data from the model output, for the years 1880–2014. While the pacemaker experiment has limitations, CMIP6 models have not significantly improved upon CMIP5 in the representation of the ASL (Bracegirdle et al. 2020). However, the pacemaker simulations have a reasonable representation of the SLP seasonal cycle, albeit biased low, and the longitude of the ASL is broadly in correspondence with that of ERA5 for JJA and DJF, with an eastward bias in MAM and SON (not shown). Most CMIP6 models have a too-weak representation of the amplitude of the teleconnection from the tropical Pacific, with a westward bias and reduced amplitude of tropical Pacific precipitation

anomalies, thought to be associated with a cold SST bias in the climatological mean (Fang et al. 2024). Using the pacemaker simulations will help to rectify this, and these simulations represent the tropical Pacific teleconnection well (Schneider and Deser 2018).

Here, we focus on the area-averaged ASL index and we calculate this for each ensemble member. Using the full length of the model (1880–2014), we calculate a sliding window correlation of successive 31-yr periods for each Southern Hemisphere grid cell between the ensemble member ASL and the member SLP field. We also calculate correlations for the whole period, which we mask, first to retain significant correlations and then to retain those correlations only for grid cells where at least 70% of the moving window correlations are significant ($p < 0.1$) for at least seven members, indicating regions with a consistent significant correlation over time across members. We use the stations lying within these "stable correlation" regions to create additional reconstructions. This approach of testing the stationarity of the reconstructed relationships is qualitatively similar to that of Clark and Fogt (2019), who performed similar pseudoreality tests using different climate model simulations.

3. Results

a. Station significance, EOF, and PC construction

Tables 1 and 2 summarize the correlations between time series of seasonal-mean SLP at individual stations and the ASL index for each season. These stations ensure the inclusion of relevant station data from the Southern Hemisphere (Fig. 3a). Of the 56 stations (63 including Antarctic stations), more are used in the 1957 models, due to a higher number of stations having data available for this period. At most, just over half of the available stations have significant correlations with the ASL (e.g., 40 stations used for the 1957 ANT+ reconstruction at the $p < 0.1$ significance level; Table 3). In contrast, as few as seven stations are used in the longer reconstructions starting in 1905 (MAM, $p < 0.05$, Table 3).

Figure 3 presents an example of the station loadings onto the EOFs, for the SON area-averaged ASL index only at the $p < 0.1$ significance level. Loadings are similar for $p < 0.05$ but generally with fewer stations selected. Loadings for the ANT+ reconstructions are not shown. The EOFs show broadly similar loading patterns, irrespective of the time period of the reconstruction, except that longer time series has fewer stations contributing to the EOFs. For EOF1 of any time period, all loadings are of the same sign and dominated by stations in South America and New Zealand. For EOF2 (1957 and 1905 only), a dipole is evident, with positive loadings in South America and negative in New Zealand. Tahiti (17.6°S, 149.6°W) changes its loading sign between 1957 (negative) and 1905 (positive), which is likely due to IPO decadal-scale variability.

Most reconstructions are based on one or two PCs, with three PCs used in 6 of the 32 seasonal reconstructions (Table 3). Three PCs are used in the longer (1905 and 1941) reconstructions only. In MAM, SON, and DJF, PC1 is always used, whereas in JJA, in three reconstructions (1957 $p < 0.05$, 1957 $p < 0.1$, and 1957 ANT+ $p < 0.1$), PC1 is not used, with PC2 being the most frequently used PC.

TABLE 2. As in Table 1, but for the additional Antarctic stations. A number of other stations have data, but they either have large gaps or start after 1957. All stations significant at $p < 0.05$.

Station	Availability	MAM	JJA	SON	DJF
Esperanza	1957–2023	0.37	0.49	0.68	0.81
Amundsen–Scott	1957–2023	0.32	0.39	0.6	0.72
Halley	1957–2023	0.5	0.47	0.69	0.87
Vernadsky	1957–2023	0.43	0.54	0.7	0.84
Mawson	1957–2023	0.49	0.6	0.7	0.84
Mirny	1957–2023	0.43	0.4	0.58	0.73
Casey	1957–2023	0.43	0.45	0.57	0.73

To explore the association of loading patterns with the SLP field, we regress the significant PCs for the 1957 reconstructions onto the detrended SLP standardized anomaly field for the fitting period (Fig. 4). Evidence of tropical Pacific teleconnections, with nodes of alternating sign over New Zealand, the Amundsen Sea, and southern South America, is present in MAM (PC1), JJA (PC2), and SON (PC1). JJA PC1 is characterized by an east–west dipole (not shown). However, DJF PC1 shows a more zonal pattern, consistent with wave reflection by the background winds limiting wave train propagation to the Amundsen Sea in this season (Li et al. 2021). The PC4 patterns for MAM and JJA exhibit a discernible zonal wavenumber-3 component. For MAM (Fig. 1b arrow), the PC4 pattern resembles the tropical Atlantic wave train (Li et al. 2021; their Fig. 1c). While some similarities to this wave train are evident for JJA, the pattern is less prominent. In SON, PC3 most resembles this pattern (not shown) but is never selected as a significant predictor PC (Table 3), while SON PC2 is more like zonal wavenumber 1 and DJF PC3 again shows a near-zonal pattern.

b. Reconstructions of the ASL index

We have produced an ensemble of eight reconstructions over different time periods, using two significance thresholds. Only two reconstructions cover 1905–40, while for 1941–56, there are four, and from 1957 onward, there are eight reconstructions. We calculate an ensemble mean for each season from these reconstructions. We compare the reconstructions with ASL indices from ERA5 (1940–2023), 20CRv3 (1905–2015), and ModE-RA (1905–2008) (Fig. 5), and statistics for the fitting period for the leave-one-out cross validation are presented in Table 4.

The R^2 values range from 0.29 (MAM, 1957, $p < 0.05$) to 0.83 (SON 1957 ANT+, $p < 0.05$, Table 4). Overall, the best model fit (high R^2 and correlation and low MAE and RMSE) is for DJF and the poorest for MAM. The poorer MAM performance is not attributable to fewer predictor stations, as the number is similar to JJA (Table 1). While correlations between the ASL and South American stations are higher in MAM than in JJA, correlations with New Zealand stations are lower (−0.26 to −0.41 in MAM and −0.33 to −0.57 in JJA; Table 1). This reflects the fact that the MAM significant correlations of ASL with Southern Hemisphere SLP are notably contracted and weaker over this region (Fig. 2a), i.e., a weaker teleconnection strength. The New Zealand region is a key predictor

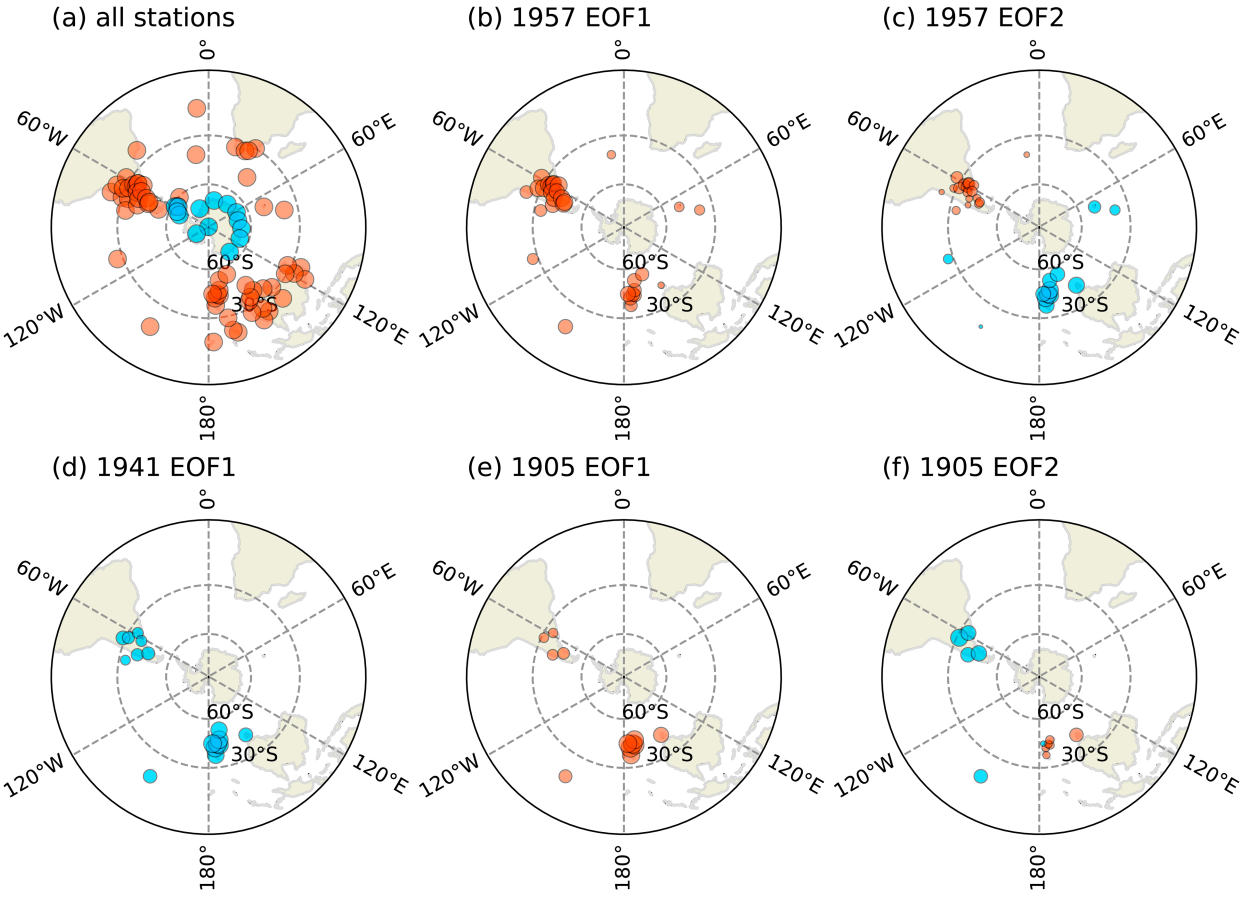

FIG. 3. (a) Stations available for the analysis, Antarctic = blue and lower latitudes = orange; (b)–(f) SON station loadings for significant ($p < 0.1$) EOFs for the different reconstruction lengths. (b)–(f) The size of the circle is proportional to the loading of the station; positive loadings are orange, and negative loadings are blue. Note that in (c), Tahiti (17.6°S, 149.6°W) is blue, but the weighting is too small to allow the color to be seen clearly.

region, with high correlations with the ASL in all seasons and long station SLP records. New Zealand is south of the South Pacific convergence zone and located under one of the nodes on the teleconnection wave train to Antarctica from this region (Clem et al. 2019; their Fig. 2a). New Zealand stations are likely to capture some of this signal, but it appears weaker in MAM.

Adding the Antarctic stations improves the fit across all seasons, but as these are only consistently available post-1957, longer reconstructions must rely on lower-latitude station data. It is notable that increasing the number of stations does not necessarily add much improvement to the model fit. The 1905 model statistics where fewer than 15 stations are used are not greatly different from those for 1957, without the Antarctic stations,

TABLE 3. The number of PCs used in each reconstruction of the ASL area-averaged index and the number of significant stations used to construct the EOFs. The PCs used in the reconstruction are shown in square brackets.

	MAM		JJA		SON		DJF	
Model	PCs	Stations	PCs	Stations	PCs	Stations	PCs	Stations
1957 *p*0.1	2 [1, 4]	27	2 [2, 4]	26	2 [1, 2]	32	2 [1, 3]	33
1957 *p*0.05	1 [1]	20	1 [2]	15	2 [1, 2]	31	1 [1]	25
1957 *p*0.1 ANT+	2 [1, 4]	34	1 [2]	33	3 [1, 2, 4]	39	1 [1]	40
1957 *p*0.05 ANT+	2 [1, 4]	27	2 [1, 2]	22	2 [1, 2]	38	1 [1]	32
1905 *p*0.1	3 [1, 2, 4]	8	3 [1, 2, 4]	13	2 [1, 2]	12	3 [1, 2, 4]	10
1905 *p*0.05	2 [1, 2]	7	2 [1, 2]	10	1 [1]	12	3 [1, 2, 3]	7
1941 *p*0.1	3 [1, 3]	15	3 [1, 4, 8]	17	1 [1]	16	2 [1, 2]	16
1941 *p*0.05	2 [1, 2]	12	2 [1, 2]	12	1 [1]	15	3 [1, 2, 3]	13

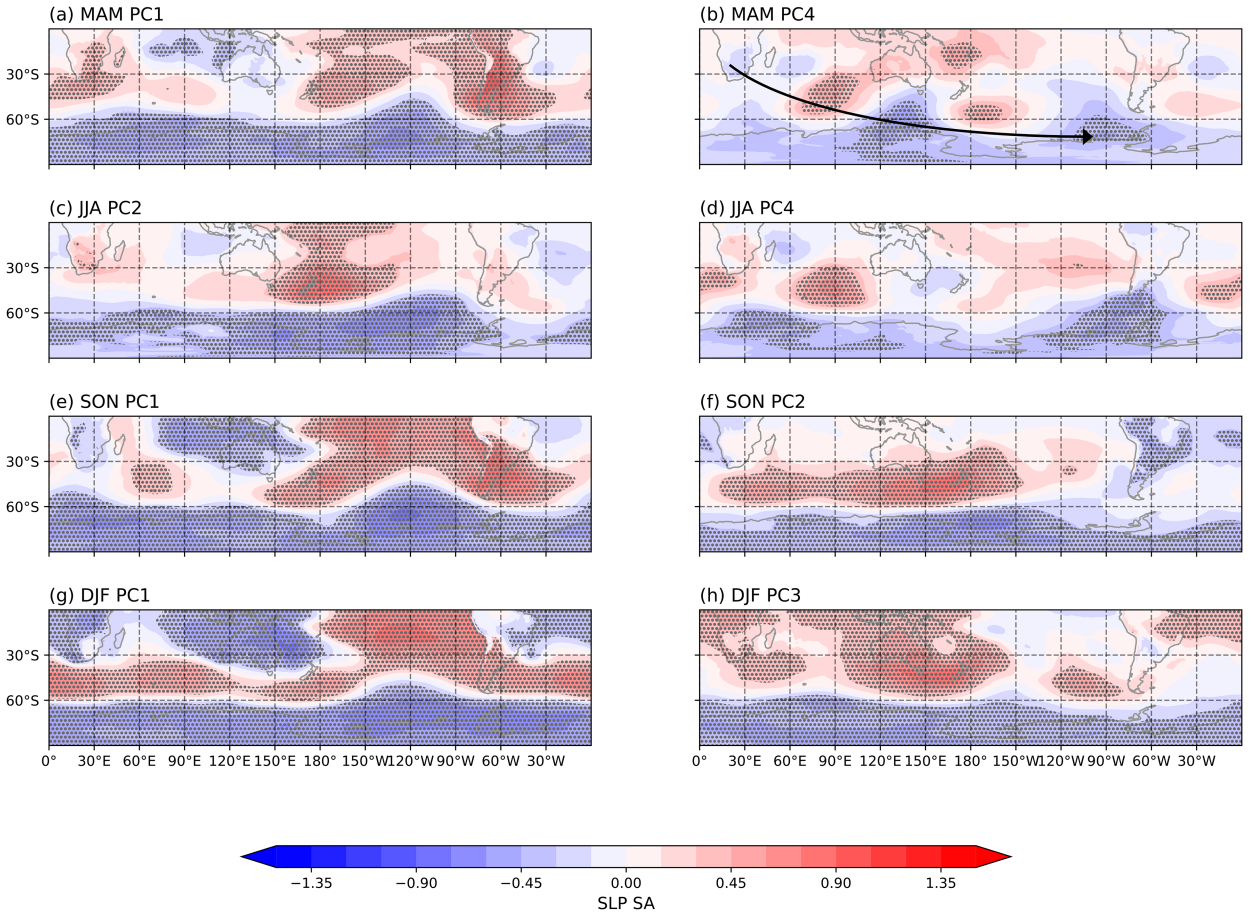

FIG. 4. Regressions of significant PCs onto SLP field. Significant PCs are taken from the 1957, $p < 0.1$ reconstructions, and the regressions are for the fitting period 1979–2023. Regions of statistical significance ($p < 0.05$) are stippled.

which use up to 33 stations (Table 3). The identification of a relatively small number of stations in key locations appears to be more important than simply including many extra stations from regions in the Southern Hemisphere which already have predictors. As a sensitivity test, six stations with a high loading onto EOFs 1 and 2 for the SON 1957 $p < 0.05$ model were selected. Three were chosen from South America (Resistencia, Ezeiza, and Santa Rosa) and three from New Zealand (Wellington, Christchurch, and Chatham Islands) to represent the two main nodes shown in Figs. 3b and 3c. These six stations alone produced a reconstruction with an R^2 value of 0.54, virtually indistinguishable from the full reconstruction using 31 stations ($R^2 = 0.56$).

SON and DJF have the best validation statistics (Table 4), due to there being larger regions over midlatitude land areas with station observations with teleconnections to the ASL in these latter two seasons (Fig. 2). Strong reconstruction potential could be expected in SON, as it is the season with the strongest tropical teleconnections (Jin and Kirtman 2009). Anomalous deep convection during strong ENSO events drives Rossby wave train propagation toward the Antarctic, following the PSA pattern, which shows seasonal variability, being most evident in SON (Schneider et al. 2012). The influence of the SAM on the ASL in DJF is evident in the more zonal patterns of SLP relating to the PCs used in the reconstruction (Figs. 4g,h). Detrended SAM–ASL correlations, using the SAM reconstruction from 1957 (Marshall 2003, updated), are −0.56 (MAM), −0.6 (JJA), −0.77 (SON), and −0.82 (DJF). Wave reflection by a strong polar front jet limits wave propagation from the tropics to the Amundsen Sea (Scott Yiu and Maycock 2019); hence, the ASL is more likely to be influenced by the SAM in DJF, when a single zonal tropospheric polar front jet (Fogt and Marshall 2020) is too strong for tropical teleconnections (Scott Yiu and Maycock 2019). In JJA, a strong subtropical jet favors a Rossby wave source with poleward-weakening winds throughout the troposphere, allowing for their propagation to Antarctica.

c. *Comparison of reconstruction with reanalyses*

The 20CRv3 ASL index is consistently more positive (a weaker ASL) than the reconstructions and the ModE-RA reanalysis ASL prior to 1950 (Fig. 5), with values at the top of, or outside, the uncertainty range of the reconstructions. This high-pressure bias is likely as the model is less constrained by the very few observations in the early half of the twentieth century, in agreement with early twentieth-century high-pressure biases in the Southern Hemisphere in 20CRv3 and other

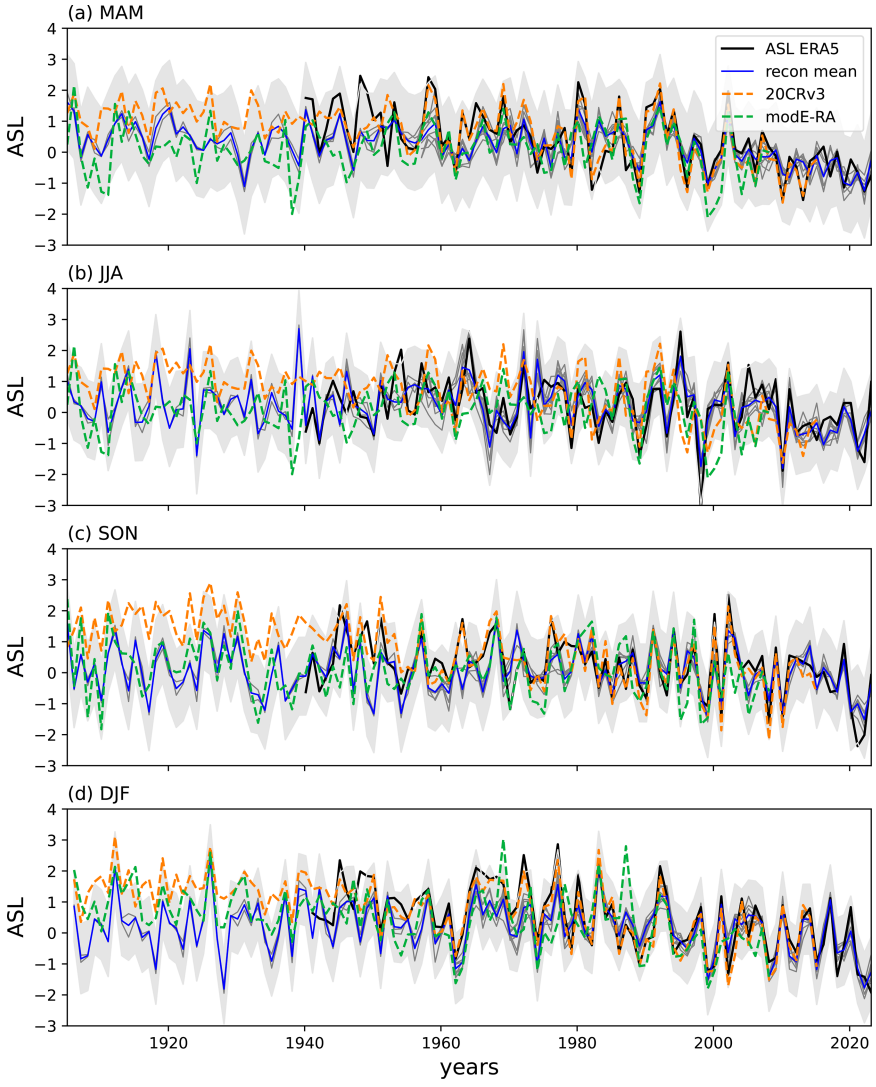

FIG. 5. The reconstructed area-averaged ASL indices. Individual reconstructions starting at different times are shown as gray lines, and the mean of this ensemble is shown in blue. The gray shading denotes ±1.96 SD of the residuals added/subtracted from the ensemble mean for the fitting period (1979–2023). The ERA5 ASL index is in black, the ASL index from the 20CRv3 is in dashed orange, and the ASL index from ModE-RA is dashed green.

historical reanalyses found in other studies (Schneider and Fogt 2018; Fogt et al. 2021). However, despite this difference in means, the interannual correlation between the reconstruction mean and 20CRv3 over the reconstruction period is significant ($p < 0.01$) and in all seasons except SON is 0.67 or 0.68 (Table 5). Correlations between the reconstruction and ModE-RA ensemble mean ASL for 1905–2008 are also high, and the time series does not show the positive biases evident in 20CRv3. Interestingly, prior to the period of assimilated satellite observations (and prior to the fitting period), the ERA5 ASL index is also more positive than the reconstructed ASL, in particular in MAM and SON. Correlations between 20CRv3 and ModE-RA are lower than those between the reconstruction mean and reanalyses, except for DJF.

d. Variability of correlations between the reconstruction and reanalyses

To explore the strength of agreement through time between our reconstructed ASL index and the ASL indices from the three different reanalyses, we calculate 31-yr moving window correlations between each index pair (Fig. 6). Overall, the majority of moving window correlations are significant ($p < 0.05$) and generally increase toward the present but with considerable decadal variation. Examining the correlations between reanalyses first (dashed lines), in each season from the 1950s, the correlations between 20CRv3 and ERA5 are highest. The correlations between ModE-RA and the other reanalyses (20CRv3 and ERA5) match very closely, particularly

TABLE 4. Validation statistics for the eight reconstructions, comparing the cross-validated fit with ERA5, 1979–2023. Corr = Pearson correlation; MAE = mean absolute error; RMSE = root-mean-square error. The range of values across the models is shown. Bold numbers indicate the best statistics for each season (highest R^2 and correlation and lowest MAE and RMSE).

	MAM				JJA				SON				DJF			
Model	R^2	Corr	MAE	RMSE	R^2	Corr	MAE	RMSE	R^2	Corr	MAE	RMSE	R^2	Corr	MAE	RMSE
1957 p0.1	0.33	0.58	0.66	0.81	0.62	0.79	0.48	0.61	0.57	0.75	0.48	0.65	0.59	0.77	0.53	0.63
1957 p0.05	0.29	0.55	0.69	0.83	0.49	0.7	0.53	0.71	0.56	0.75	0.48	0.65	0.65	0.81	0.49	0.59
1957 p0.1 ANT	**0.53**	**0.73**	**0.52**	**0.68**	0.66	0.81	0.44	0.57	**0.75**	**0.87**	**0.36**	**0.49**	0.77	0.88	0.38	0.47
1957 p0.05 ANT	0.52	0.72	**0.52**	0.69	**0.71**	**0.84**	**0.42**	**0.53**	0.68	0.82	0.42	0.56	**0.83**	**0.91**	**0.33**	**0.41**
1905 p0.1	0.37	0.61	0.64	0.79	0.63	0.79	0.47	0.6	0.56	0.75	0.5	0.66	0.56	0.75	0.52	0.66
1905 p0.05	0.32	0.56	0.68	0.82	0.52	0.72	0.53	0.68	0.47	0.68	0.56	0.72	0.6	0.77	0.49	0.63
1941 p0.1	0.32	0.57	0.66	0.81	0.59	0.77	0.49	0.64	0.55	0.74	0.5	0.66	0.62	0.79	0.52	0.61
1941 p0.05	0.36	0.6	0.66	0.79	0.54	0.74	0.52	0.67	0.54	0.73	0.51	0.67	0.68	0.83	0.44	0.56
Range	0.29–0.53	0.55–0.73	0.52–0.69	0.68–0.83	0.49–0.71	0.7–0.84	0.42–0.53	0.53–0.71	0.47–0.75	0.68–0.87	0.36–0.56	0.49–0.72	0.56–0.83	0.75–0.91	0.33–0.53	0.41–0.66

after 1970. From around 1970, correlations between the ASL indices for 20CRv3 and ERA5 are very high in all seasons, indicating that while 20CRv3 includes no satellite observations, the increased number of SLP observations alone is sufficient to well constrain the ASL index. The ModE-RA ASL index agrees less well with the other two reanalysis indices over this period, likely due to no additional series of observations being added to ModE-RA after 1890 (Valler et al. 2024).

Correlations between our reconstruction and the reanalyses (solid lines), from around 1970, in MAM, JJA, and SON broadly increase toward the present. In MAM, the correlations between our reconstruction and both reanalyses are lower in the early twentieth century and are sometimes insignificant for 20CRv3. This reflects the poorer model-fitting statistics of our MAM reconstruction (Table 4), but given that agreement between ModE-RA and 20CRv3 is also low, it indicates perhaps that in this season the ASL is less well constrained by the tropical teleconnections (see section 3b) and possible fluctuations in the strength of the association between the teleconnection and the ASL.

For JJA and SON, correlations between the reconstruction and 20CRv3 (green line) are lowest for windows centered in the mid-twentieth century but stronger prior to this. This may be partly related to the amount of data assimilated, as the steep drop in correlations may relate to a reduction in ships sailing around Cape Horn after the opening of the Panama Canal in 1914, the period post the assimilation of data from Heroic Expeditions (Edinburgh and Day 2016; Fogt et al. 2021), and the end of the window covering World War II (WWII). However, this seems unlikely to be purely related to the amount of data assimilated as the low correlations extend into season windows centered in the 1960s and 1970s. Another explanation may be that the North Atlantic Oscillation (NAO) (Weisheimer et al. 2017; O'Reilly et al. 2017) and ENSO (Weisheimer et al. 2020; Wright et al. 2024) have lower predictability in the mid-twentieth century, linked to lower persistence in tropical Pacific SST anomalies and a less variable ENSO (Wright et al. 2024). This impact on Northern Hemisphere teleconnections may also have a similar effect on Southern Hemisphere teleconnections and contribute to weaker associations between station SLP and the ASL during such periods. Another possibility is that the variation in correlation is simply due to internal variability of the atmosphere–ocean system (e.g., Weisheimer et al. 2020) and that correlations, while variable, are still mostly significant. Whatever the cause, there is increased uncertainty in the ASL indices in the mid-twentieth century.

In DJF, correlations between the reconstruction, 20CRv3, and ModE-RA are more consistent throughout the twentieth century, suggesting less dependence on the tropical teleconnections in this season, combined with higher numbers of observations assimilated in the reanalyses at higher latitudes in DJF (Slivinski et al. 2019). This is supported by the more zonal patterns seen in Fig. 4, where the selected PCs are not associated with tropical teleconnections. For all seasons, the correlations between the reconstruction and ModE-RA show

TABLE 5. Correlations for each season between 20CRv3, reconstruction mean, and ModE-RA area-averaged ASL indices. All correlations are highly significant ($p < 0.01$). 1905–2008 correlations between the reconstruction and 20CRv3 are given in square brackets, to allow direct comparison with ModE-RA correlations.

Season	20CRv3/ reconstruction 1905–2015 [1905–2008]	20CRv3/ ModE-RA 1905–2008	Reconstruction/ ModE-RA 1905–2008
MAM	0.68 [0.64]	0.50	0.63
JJA	0.67 [0.62]	0.44	0.67
SON	0.54 [0.54]	0.53	0.67
DJF	0.67 [0.63]	0.65	0.61

less decadal variation than correlations with the other two reanalyses.

e. *Lower-frequency variability*

To examine lower frequency rather than interannual variability in the reconstructions, we smooth the century-length ASL indices with a 7-yr Hamming window (Fig. 7). The choice of smoothing method can affect the timing and amplitude of changes. We checked sensitivity to this by using a 7-yr low-pass Butterworth filter and found that this produces qualitatively similar results, with similar timings but increased amplitude: The amplitude changes are nonetheless consistent through the series, suggesting our particular choice of smoothing does not impact our main conclusions. The smoothed version captures ENSO time-scale variability while removing interannual variability. The early twentieth-century high-pressure bias (too weak ASL) in 20CRv3 is very clear in all seasons (Fig. 7, left column) and is particularly prominent in JJA and SON. ModE-RA shows no such bias in MAM and SON, with a smaller bias in DJF prior to 1940 (Fig. 7g). In JJA, ModE-RA shows a more negative ASL index (stronger ASL) prior to the 1970s including strong negative periods in the 1920s and 1940s that are not present/as pronounced in our reconstruction (Fig. 7c).

The filtered values also help to clarify the recent negative trends in the ASL, which are present in all seasons but are least evident in SON (Fig. 7e). The smoothed time series confirms the unsuitability of 20CRv3 reanalysis for analyzing longer-term trends due to the high-pressure bias in the early twentieth century (section 1). In all seasons, current filtered values of our reconstruction show the deepest ASL in the series, even if individual years are not the deepest (Fig. 5b; JJA ASL is deepest in 1923). Although the ModE-RA data do not extend to the present, the ASL around 2000 appears to be one of the deepest in the series in all seasons except SON.

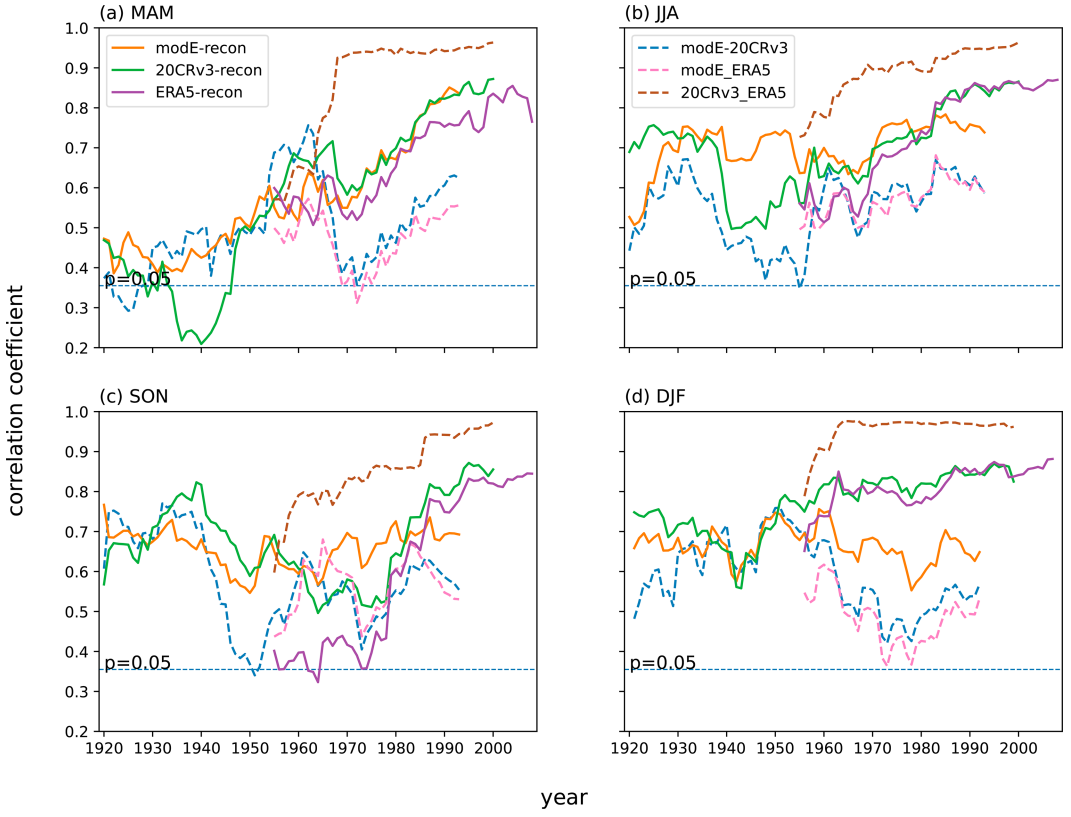

FIG. 6. 31-yr running correlations between the reconstruction mean ASL and reanalyses for each season. The year of the window is the central year. The $p = 0.05$ significance threshold is shown as a horizontal dashed line. (b) Dashed lines show correlations between reanalyses, and (a) solid lines show the correlations between the reconstruction and the different reanalyses.

FIG. 7. ASL depth time series smoothed with a 7-yr Hamming filter, for the reconstruction mean, ModE-RA, and the 20CRv3. (a),(c),(e),(g) The filtered series and (b),(d),(f),(h) the filtered series adjusted by linearly detrending and renormalizing.

To better compare the timing of decadal variability, we further process the time series by linearly detrending the filtered time series and restandardize by removing the mean of the series for the whole time period and dividing by the standard deviation (Rakthanmanon et al. 2013) (Figs. 7b,d,f,h). For each season, there are periods where the standardized decadal variability of all three indices is very similar, where we may have increased confidence that this is a reasonable representation of ASL variability. For example, in DJF, there is a clear deep ASL in all indices just after 1960, with a weak ASL in the late 1960s (Fig. 7h). In MAM, there is broad agreement between the three indices between 1945 and 1980 (Fig. 7b).

Furthermore, in SON, DJF, and to a lesser extent JJA, all three indices show high ASL values (i.e., a weaker ASL) around 1930 and in the early 1940s, with low values/a strong ASL centered on 1935 (Figs. 7d,f,h), in agreement with annual ASL index reconstructions (Dalaiden et al. 2021; O'Connor et al. 2021; Fig. S2), which is identified as originating in tropical forcing (Ding et al. 2011, 2012; Dalaiden et al. 2024). Warming in West Antarctica from 1936 to 1945 was associated with a persistent El Niño event during 1940–42 (Schneider and Steig 2008; Brönnimann et al. 2004). Around this time, the Pine Island Glacier started to retreat (Smith et al. 2017), confirmed from sedimentological observations. Enhanced westerlies at the continental shelf break (a weaker ASL) are consistent with enhanced CDW transport under the ice shelf (Steig et al. 2012, 2013). From annual reconstructions, Holland et al. (2022) identified westerly wind anomalies at the shelf break during this period, although the magnitudes of these trends were found not to be extreme (O'Connor et al. 2023).

f. Trends

We calculate time-varying linear trends for periods greater than 20 years (Fig. 8). For our reconstruction, there is clear decadal and multidecadal variability in the trends of all four seasons, with periods of both positive (albeit mostly insignificant) and negative trends, mostly present along the diagonal line. In contrast, 20CRv3 trends are dominantly negative (a strengthening of the ASL) over most time scales, due to the early twentieth-century high-pressure bias. Positive trends (a weakening of the ASL) starting for years in the mid-twentieth century are evident in all seasons in both the reconstruction and ModE-RA, although those in DJF are for a shorter range of window start dates/lengths, where the trends resemble those in 20CRv3. This is because the DJF ModE-RA ASL index is higher than the reconstruction over the first part of the twentieth century (Fig. 7d) and so has more extensive negative trends at different time scales, although fewer of these trends are significant compared to those in 20CRv3. The positive DJF trend, which is present in all three datasets (although

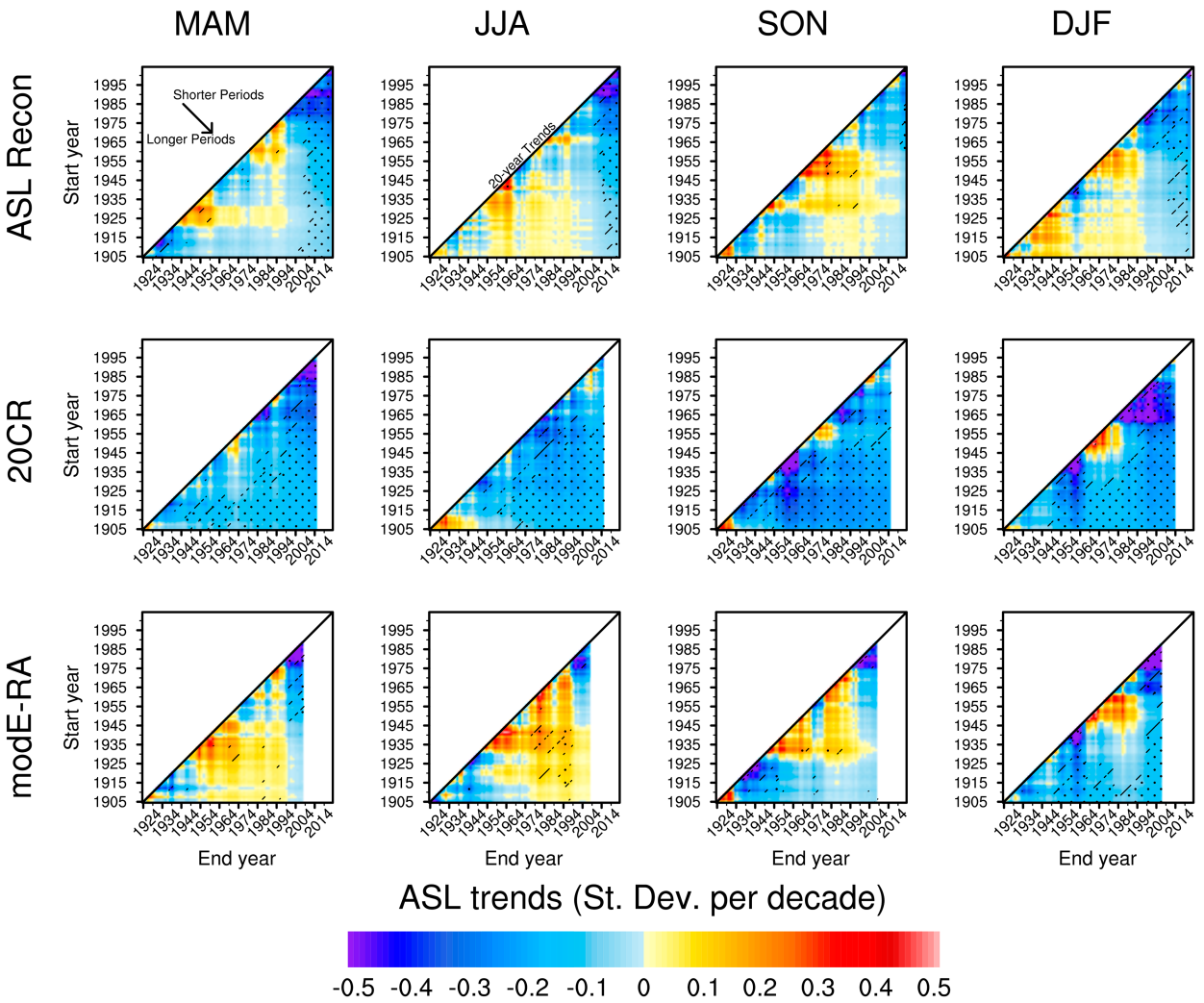

FIG. 8. Time-varying linear trends of the reconstructed ASL mean index and the ASL indices from 20CRv3 and ModE-RA, for each season. The y axis is the start year for each trend, and the x axis is the end year. Trend periods get longer toward the bottom right of each plot. The diagonal line is equivalent to 20 years, and trends are only shown for periods longer than 20 years. The hatching and stippling show trends that are significantly different from zero at $p < 0.1$ and $p < 0.05$, respectively, based on the Student's t test.

only significant in ModE-RA), stems from a deep ASL in ~1961, which is a robust feature in all three series (Figs. 7g,h).

In the SON reconstruction, there are significant positive trends starting during the abovementioned period of deep ASL in the 1930s over periods of 30–50 years, which are also present in ModE-RA. The MAM and JJA reconstructions show limited significant 30-yr positive trends from around 1930 (JJA) and 1925 and 1960 (MAM).

The recent deepening of the ASL (a more negative index) is seen in all seasons in significant negative trends in our reconstruction (upper right corners of each panel in the top row of Fig. 8). These negative trends also extend over the whole time period for MAM, JJA, and DJF (bottom right of each panel). These three seasons have a more marked recent strengthening of the ASL, although shorter trends starting in the early part of the time series (bottom left of each panel) are not significant, indicating that the shift toward a more negative ASL index occurred in the latter part of the twentieth century. In SON, the recent negative trends are less pronounced (Figs. 5c and 7c) but are significant from around 1950. 20CRv3 shows little multidecadal variability in the sign of the trends, although at shorter time scales (trends of 20–30 years, where the significance is less clear), particularly in SON and DJF, there is some evidence of positive trends around the mid-twentieth century. The unprecedented nature of recent significant negative trends within the time frame of the reconstruction is confirmed by a separate analysis of 21- and 31-yr trends using the nonparametric Mann–Kendall test (Fig. S3), accounting for serial autocorrelation.

Our reconstructions allow us to explore the seasonality of the recent deepening of the ASL in a longer-term perspective, which is not possible using 20CRv3 due to its early twentieth-century pressure bias. Annual reconstructions of the twentieth-century ASL from O'Connor et al. (2021) and Dalaiden et al. (2021) are based on proxy information (Fig. S2). The O'Connor

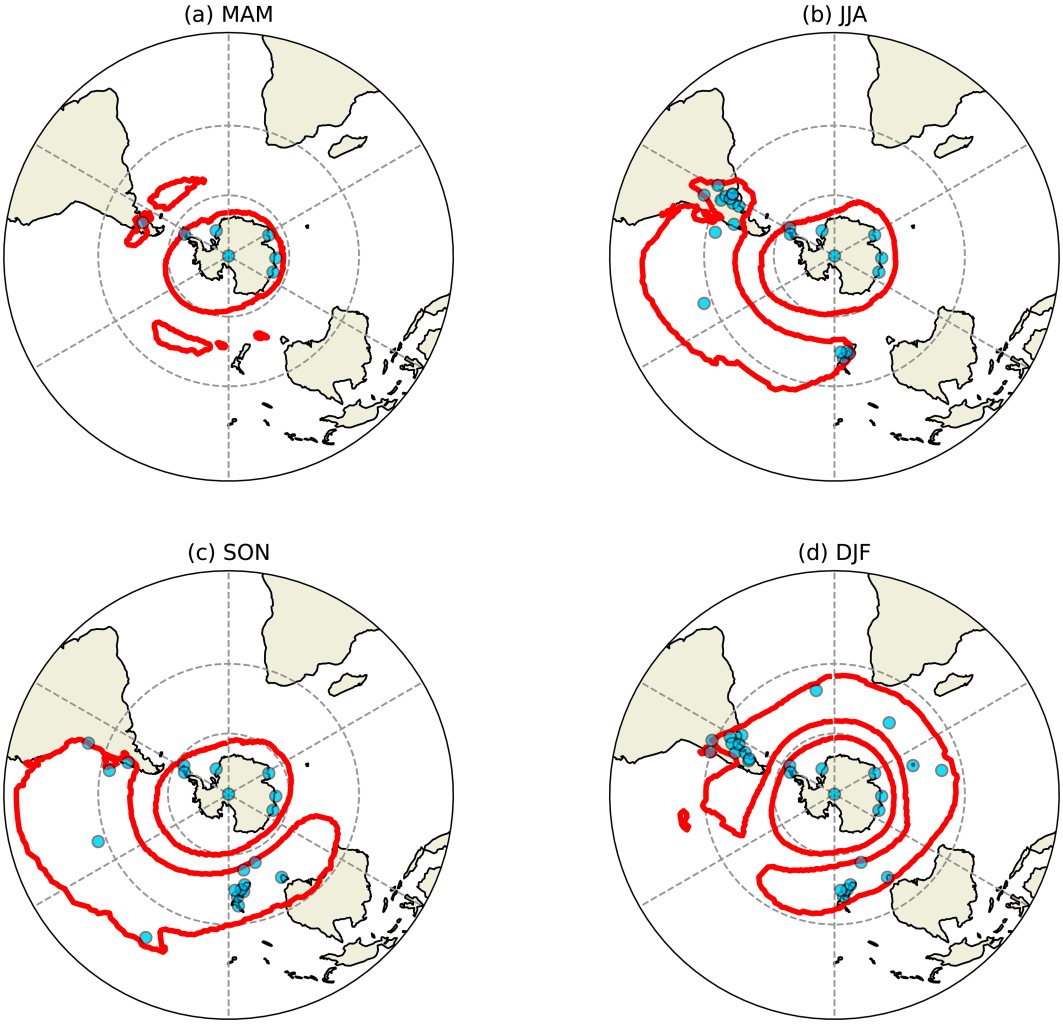

FIG. 9. Regions of stable correlations with ASL from the 10 members of the pacemaker simulations. The red contours enclose regions where at least 70% of 31-yr running correlations are significant, for at least seven of the ensemble members. Blue circles show the locations of stations lying within the stable correlation region.

index shows a deepening (negative trend) of the ASL during the twentieth century, whereas the Dalaiden index shows no trend from 1850 to 1950, with a subsequent negative trend post-1950. In our reconstruction, the strongest significant negative trends start from the mid-1970s, which, particularly in MAM and JJA, indicate that the recent deepening of the ASL (Turner et al. 2013) is unprecedented over the period of the reconstruction. The ModE-RA reanalysis, which includes proxy, documentary, and instrumental data, only extends to 2008 but shows recent deepening of the ASL in all seasons and positive mid-century trends in broad agreement with our reconstruction. This more recent deepening of the ASL has been attributed to the influence of anthropogenic forcing (greenhouse gases and stratospheric ozone; Holland et al. 2022; Dalaiden et al. 2022).

g. *Stability of reconstructions*

An assumption of the PCR reconstruction approach is that associations between station pressure and the ASL remain stable over time. This cannot be verified from modern reanalysis data such as ERA5 as the time series of reliable data is too short (post-1979 only for the satellite period). One way of assessing the stability of these teleconnections is by using the Pacific pacemaker ensemble, using sliding window correlations (section 2d). Regions where stable significant correlations between SLP and the ASL are identified are shown in Fig. 9.

In MAM, there is only a single station outside Antarctica that lies within a stable region (Fig. 9a). It is not possible to do a reconstruction using stations in regions of stable teleconnections for this season, except by using Antarctic stations only, which are only available from 1957 and do not capture any of the important Southern Hemisphere teleconnections. The reconstructions for MAM prior to 1957 should therefore be interpreted with caution as the temporal nonstationarity suggests reconstructions calibrated during different periods would yield different reconstructions (and included stations). The stable region outside the Antarctic in JJA and SON is focused on the South

TABLE 6. Validation statistics for the eight reconstructions using only stations from the stable regions identified in Fig. 9, comparing the cross-validated fit with ERA5, 1979–2023. Corr: Pearson correlation; MAE: mean average error; RMSE: root-mean-square error. The range of values across the models is shown.

	JJA				SON				DJF			
Model	R^2	Corr	MAE	RMSE	R^2	Corr	MAE	RMSE	R^2	Corr	MAE	RMSE
1957 p0.1	0.4	0.63	0.63	0.77	0.43	0.66	0.57	0.74	0.46	0.68	0.58	0.73
1957 p0.05	0.46	0.68	0.54	0.72	0.44	0.66	0.56	0.74	0.51	0.72	0.57	0.69
1957 p0.1 ANT	0.67	0.82	0.44	0.57	0.75	0.86	0.38	0.5	0.7	0.84	0.44	0.55
1957 p0.05 ANT	0.65	0.81	0.45	0.58	0.71	0.84	0.4	0.53	0.76	0.87	0.4	0.49
1905 p0.1	0.43	0.65	0.61	0.75	0.46	0.68	0.56	0.73	0.33	0.58	0.62	0.81
1905 p0.05	0.45	0.67	0.57	0.74	0.41	0.64	0.59	0.76	0.36	0.6	0.62	0.79
1941 p0.1	0.42	0.65	0.55	0.75	0.49	0.7	0.57	0.71	0.46	0.68	0.59	0.73
1941 p0.05	0.48	0.69	0.55	0.71	0.42	0.65	0.58	0.75	0.38	0.62	0.61	0.78
Range	0.40–0.67	0.63–0.82	0.44–0.63	0.57–0.77	0.41–0.75	0.64–0.86	0.38–0.59	0.50–0.76	0.33–0.76	0.58–0.87	0.40–0.62	0.49–0.81

Pacific, with a westward extension south of Australia evident in the latter (Figs. 9c,d). In DJF, a more circumpolar stable region is identified, consistent with wave reflection by the strong polar front jet in the South Pacific, limiting the wave train progression to the Amundsen Sea (Scott Yiu and Maycock 2019) and possibly different teleconnection patterns in this season. Ciasto et al. (2015) identify a SAM-like response in DJF to east Pacific SST anomalies; Scott Yiu and Maycock (2019) in addition find the subtropical jet wave source in this season is largely absent. Table 6 shows the validation statistics for reconstructions using only the stations identified as lying within stable correlation regions (Fig. 9), and the reconstructions are shown in Fig. S1.

In general, the validation statistics are slightly poorer for the "stable" reconstructions, although for JJA and SON, the statistics for the ANT+ reconstructions are similar to or slightly better than those in the full reconstructions. While the fit is not quite as good for the stable station reconstructions, the differences are relatively small, and fewer stations are used (Table S2). Overall, the stationarity of associations between time series for the selected stations and the ASL is very good, except for MAM, and is in agreement with Clark and Fogt (2019), who find similar stability in relationships between the extratropics and Antarctica, entirely within a climate model.

h. *Potential for reconstructions of ASL latitude and longitude indices*

We also explored whether useful reconstructions of the ASL longitude and latitude indices might be possible. Validation statistics are much poorer than for the area-averaged ASL (Tables S3 and S4). While there is some skill in the reconstructions, particularly for ASL longitude in JJA and SON (R^2 = 0.3–0.46 and 0.51–0.61, respectively, and for ASL latitude in SON when Antarctic stations are considered (R^2 = 0.44), the skill is not high enough to undertake reconstructions from station SLP alone that could be used to draw meaningful conclusions on variability of these aspects of the ASL. There may be other processes (and hence, better predictors, such as lagged variables, SST, station temperature data, and expanded geographical range of stations used) that influence these indices, which can be incorporated into more complex reconstruction models, which we will consider in future work.

4. Conclusions

In this paper, to the authors' knowledge, we provide the first seasonally resolved station-based statistical reconstruction of the ASL index, extending back to 1905 for the four standard seasons and based primarily on SLP observations from midlatitude weather stations. Our reconstructions take advantage of the teleconnections that exist linking the ASL region with lower latitudes, overcoming the obstacle of limited observational data in the Amundsen Sea region, which makes field reconstructions of SLP for this region less reliable (e.g., Fogt et al. 2024).

Using the Pacific pacemaker climate model ensemble, we find that the assumption of stationarity implicit in our reconstruction approach is valid (especially outside MAM) for a number of stations. Reconstructions based on this more limited set of stations show similar skill to our initial reconstructions. The MAM reconstruction prior to 1957 is relatively poorly constrained and should be used with caution.

There is some more limited scope for reconstructing the longitude and latitude indices. Indices such as the relative central pressure cannot be reconstructed using this approach, as the index shows little association with extratropical SLP.

Our reconstruction provides valuable insights into trends and variability of the ASL since the early twentieth century. We find that the recent negative trends since around 1960–70 are unprecedented in the context of the reconstruction over this time period, based on time-varying linear trends of the unsmoothed reconstruction data. The strongest and most significant trends occur in MAM and JJA. The ModE-RA reanalysis also shows that the strongest negative trends are the most recent. However, the 20CRv3 reanalysis is not suitable for trend identification over the twentieth century due to a high-pressure bias in the early half of the century, although interannual variability correlates well with that of the reconstruction. Correlations between the reanalyses and the reconstruction are strongest post-1970 but also show some stronger correlations in the first half of the twentieth century, particularly for JJA and SON, with the weakest correlations occurring in midcentury (1940–70), indicating increased uncertainty in this period.

Our work confirms that the strengthening of the ASL in the mid-1930s, followed by weakening around the early 1940s, is a robust feature in SON but is also evident in JJA and DJF. This is an advance on the annual perspective of previous studies. While not an extreme event in terms of ASL trends and variability, our reconstruction can capture the tropical teleconnection influences in the early twentieth century.

Future work will focus on extending the reconstructions back into the nineteenth century, as well as refining the reconstruction of the longitude and latitude indices, perhaps by considering other variables. A reconstruction of ASL longitude in particular would be important in determining variability in winds, which may enhance basal ice shelf melting, influence sea ice distribution, and lead to local warming or cooling.

Acknowledgments. We thank the two anonymous reviewers whose insightful comments have improved the manuscript. We acknowledge support from the NERC project "DeCAdeS: Drivers of Oceanic Change in the Amundsen Sea," Award NE/T012625/1. We thank the Climate Variability and Change Working Group at NCAR for making the CESM2 pacemaker simulations available.

Data availability statement. All data used in this study are available online.

REFERENCES

Allan, R., and T. Ansell, 2006: A new globally complete monthly historical gridded mean sea level pressure dataset (HadSLP2): 1850–2004. *J. Climate*, **19**, 5816–5842, https://doi.org/10.1175/JCLI3937.1.

Baines, P. G., and K. Fraedrich, 1989: Topographic effects on the mean tropospheric flow patterns around Antarctica. *J. Atmos. Sci.*, **46**, 3401–3415, https://doi.org/10.1175/1520-0469(1989)046<3401:TEOTMT>2.0.CO;2.

Barrett, H. G., J. M. Jones, and G. R. Bigg, 2018a: Reconstructing El Niño Southern Oscillation using data from ships' logbooks, 1815–1854. Part I: Methodology and evaluation. *Climate Dyn.*, **50**, 845–862, https://doi.org/10.1007/s00382-017-3644-7.

——, ——, and ——, 2018b: Reconstructing El Niño Southern Oscillation using data from ships' logbooks, 1815–1854. Part II: Comparisons with existing ENSO reconstructions and implications for reconstructing ENSO diversity. *Climate Dyn.*, **50**, 3131–3152, https://doi.org/10.1007/s00382-017-3797-4.

Benjamini, Y., and Y. Hochberg, 1995: Controlling the false discovery rate: A practical and powerful approach to multiple testing. *J. Roy. Stat. Soc.*, **57B**, 289–300, https://doi.org/10.1111/j.2517-6161.1995.tb02031.x.

Bracegirdle, T. J., E. Shuckburgh, J.-B. Sallee, Z. Wang, A. J. S. Meijers, N. Bruneau, T. Phillips, and L. J. Wilcox, 2013: Assessment of surface winds over the Atlantic, Indian, and Pacific Ocean sectors of the Southern Ocean in CMIP5 models: Historical bias, forcing response, and state dependence. *J. Geophys. Res. Atmos.*, **118**, 547–562, https://doi.org/10.1002/jgrd.50153.

——, C. R. Holmes, J. S. Hosking, G. J. Marshall, M. Osman, M. Patterson, and T. Rackow, 2020: Improvements in circumpolar Southern Hemisphere extratropical atmospheric circulation in CMIP6 compared to CMIP5. *Earth Space Sci.*, **7**, e2019EA001065, https://doi.org/10.1029/2019EA001065.

Briffa, K. R., P. D. Jones, T. M. L. Wigley, J. R. Pilcher, and M. G. L. Baillie, 1986: Climate reconstruction from tree rings: Part 2, spatial reconstruction of summer mean sea-level pressure patterns over Great Britain. *J. Climatol.*, **6** (1), 1–15, https://doi.org/10.1002/joc.3370060102.

Brönnimann, S., J. Luterbacher, J. Staehelin, T. M. Svendby, G. Hansen, and T. Svenøe, 2004: Extreme climate of the global troposphere and stratosphere in 1940–42 related to El Niño. *Nature*, **431**, 971–974, https://doi.org/10.1038/nature02982.

Ciasto, L. M., G. R. Simpkins, and M. H. England, 2015: Teleconnections between tropical Pacific SST anomalies and extratropical Southern Hemisphere climate. *J. Climate*, **28**, 56–65, https://doi.org/10.1175/JCLI-D-14-00438.1.

Clark, L., and R. Fogt, 2019: Southern Hemisphere pressure relationships during the 20th century—Implications for climate reconstructions and model evaluation. *Geosciences*, **9**, 413, https://doi.org/10.3390/geosciences9100413.

Clem, K. R., and R. L. Fogt, 2013: Varying roles of ENSO and SAM on the Antarctic Peninsula climate in austral spring. *J. Geophys. Res. Atmos.*, **118**, 11 481–11 492, https://doi.org/10.1002/jgrd.50860.

——, B. R. Lintner, A. J. Broccoli, and J. R. Miller, 2019: Role of the South Pacific convergence zone in West Antarctic decadal climate variability. *Geophys. Res. Lett.*, **46**, 6900–6909, https://doi.org/10.1029/2019GL082108.

Compo, G. P., and Coauthors, 2011: The twentieth century reanalysis project. *Quart. J. Roy. Meteor. Soc.*, **137** (654), 1–28, https://doi.org/10.1002/qj.776.

——, and Coauthors, 2019: The International Surface Pressure Databank version 4. Research Data Archive at the National Center for Atmospheric Research, Computational and Information Systems Laboratory, accessed 30 May 2024, https://doi.org/10.5065/9EYR-TY90.

Connolley, W. M., 1997: Variability in annual mean circulation in Southern high latitudes. *Climate Dyn.*, **13**, 745–756, https://doi.org/10.1007/s003820050195.

Cook, E. R., D. M. Meko, D. W. Stahle, and M. K. Cleaveland, 1999: Drought reconstructions for the continental United States. *J. Climate*, **12**, 1145–1162, https://doi.org/10.1175/1520-0442(1999)012<1145:DRFTCU>2.0.CO;2.

Dalaiden, Q., H. Goosse, J. Rezsöhazy, and E. R. Thomas, 2021: Reconstructing atmospheric circulation and sea-ice extent in the West Antarctic over the past 200 years using data assimilation. *Climate Dyn.*, **57**, 3479–3503, https://doi.org/10.1007/s00382-021-05879-6.

——, A. P. Schurer, M. C. Kirchmeier-Young, H. Goosse, and G. C. Hegerl, 2022: West Antarctic surface climate changes since the mid-20th century driven by anthropogenic forcing. *Geophys. Res. Lett.*, **49**, e2022GL099543, https://doi.org/10.1029/2022GL099543.

——, N. J. Abram, H. Goosse, P. R. Holland, G. K. O'Connor, and D. Topál, 2024: Multi-decadal variability of Amundsen Sea low controlled by natural tropical and anthropogenic drivers. *Geophys. Res. Lett.*, **51**, e2024GL109137, https://doi.org/10.1029/2024GL109137.

Danabasoglu, G., and Coauthors, 2020: The Community Earth System Model Version 2 (CESM2). *J. Adv. Model. Earth Syst.*, **12**, e2019MS001916, https://doi.org/10.1029/2019MS001916.

Ding, Q., E. J. Steig, D. S. Battisti, and M. Küttel, 2011: Winter warming in West Antarctica caused by central tropical Pacific

warming. *Nat. Geosci.*, **4**, 398–403, https://doi.org/10.1038/ngeo1129.

——, ——, ——, and J. M. Wallace, 2012: Influence of the tropics on the southern annular mode. *J. Climate*, **25**, 6330–6348, https://doi.org/10.1175/JCLI-D-11-00523.1.

Dotto, T. S., and Coauthors, 2020: Control of the oceanic heat content of the Getz-Dotson Trough, Antarctica, by the Amundsen Sea Low. *J. Geophys. Res. Oceans*, **125**, e2020JC016113, https://doi.org/10.1029/2020JC016113.

Edinburgh, T., and J. J. Day, 2016: Estimating the extent of Antarctic summer sea ice during the Heroic Age of Antarctic exploration. *Cryosphere*, **10**, 2721–2730, https://doi.org/10.5194/tc-10-2721-2016.

England, M. R., L. M. Polvani, K. L. Smith, L. Landrum, and M. M. Holland, 2016: Robust response of the Amundsen Sea Low to stratospheric ozone depletion. *Geophys. Res. Lett.*, **43**, 8207–8213, https://doi.org/10.1002/2016GL070055.

Fang, Y., J. A. Screen, X. Hu, S. Lin, N. C. Williams, and S. Yang, 2024: CMIP6 models underestimate ENSO teleconnections in the Southern Hemisphere. *Geophys. Res. Lett.*, **51**, e2024GL110738, https://doi.org/10.1029/2024GL110738.

Fogt, R. L., and E. A. Zbacnik, 2014: Sensitivity of the Amundsen Sea low to stratospheric ozone depletion. *J. Climate*, **27**, 9383–9400, https://doi.org/10.1175/JCLI-D-13-00657.1.

——, and A. J. Wovrosh, 2015: The relative influence of tropical sea surface temperatures and radiative forcing on the Amundsen Sea low. *J. Climate*, **28**, 8540–8555, https://doi.org/10.1175/JCLI-D-15-0091.1.

——, and G. J. Marshall, 2020: The Southern Annular Mode: Variability, trends, and climate impacts across the Southern Hemisphere. *Wiley Interdiscip. Rev.: Climate Change*, **11**, e652, https://doi.org/10.1002/wcc.652.

——, A. J. Wovrosh, R. A. Langen, and I. Simmonds, 2012: The characteristic variability and connection to the underlying synoptic activity of the Amundsen-Bellingshausen Seas Low. *J. Geophys. Res.*, **117**, D07111, https://doi.org/10.1029/2011JD017337.

——, C. A. Goergens, M. E. Jones, G. A. Witte, M. Y. Lee, and J. M. Jones, 2016a: Antarctic station-based seasonal pressure reconstructions since 1905: 1. Reconstruction evaluation. *J. Geophys. Res. Atmos.*, **121**, 2814–2835, https://doi.org/10.1002/2015JD024564.

——, J. M. Jones, C. A. Goergens, M. E. Jones, G. A. Witte, and M. Y. Lee, 2016b: Antarctic station-based seasonal pressure reconstructions since 1905: 2. Variability and trends during the twentieth century. *J. Geophys. Res. Atmos.*, **121**, 2836–2856, https://doi.org/10.1002/2015JD024565.

——, C. P. Belak, J. M. Jones, L. C. Slivinski, and G. P. Compo, 2021: An assessment of early 20th century Antarctic pressure reconstructions using historical observations. *Int. J. Climatol.*, **41**, E672–E689, https://doi.org/10.1002/joc.6718.

——, A. M. Sleinkofer, M. N. Raphael, and M. S. Handcock, 2022: A regime shift in seasonal total Antarctic sea ice extent in the twentieth century. *Nat. Climate Change*, **12**, 54–62, https://doi.org/10.1038/s41558-021-01254-9.

——, Q. Dalaiden, and G. K. O'Connor, 2024: A comparison of South Pacific Antarctic Sea ice and atmospheric circulation reconstructions since 1900. *Climate Past*, **20**, 53–76, https://doi.org/10.5194/cp-20-53-2024.

Goyal, R., M. Jucker, A. Sen Gupta, and M. H. England, 2021: Generation of the Amundsen Sea low by Antarctic orography. *Geophys. Res. Lett.*, **48**, e2020GL091487, https://doi.org/10.1029/2020GL091487.

Hannaford, M. J., J. M. Jones, and G. R. Bigg, 2015: Early-nineteenth-century southern African precipitation reconstructions from ships' logbooks. *Holocene*, **25**, 379–390, https://doi.org/10.1177/0959683614557573.

Henley, B. J., J. Gergis, D. J. Karoly, S. Power, J. Kennedy, and C. K. Folland, 2015: A tripole index for the interdecadal Pacific oscillation. *Climate Dyn.*, **45**, 3077–3090, https://doi.org/10.1007/s00382-015-2525-1.

Hersbach, H., and Coauthors, 2020: The ERA5 global reanalysis. *Quart. J. Roy. Meteor. Soc.*, **146**, 1999–2049, https://doi.org/10.1002/qj.3803.

Holland, P. R., T. J. Bracegirdle, P. Dutrieux, A. Jenkins, and E. J. Steig, 2019: West Antarctic ice loss influenced by internal climate variability and anthropogenic forcing. *Nat. Geosci.*, **12**, 718–724, https://doi.org/10.1038/s41561-019-0420-9.

——, and Coauthors, 2022: Anthropogenic and internal drivers of wind changes over the Amundsen Sea, West Antarctica, during the 20th and 21st centuries. *Cryosphere*, **16**, 5085–5105, https://doi.org/10.5194/tc-16-5085-2022.

Hosking, J. S., A. Orr, G. J. Marshall, J. Turner, and T. Phillips, 2013: The influence of the Amundsen–Bellingshausen Seas low on the climate of West Antarctica and its representation in coupled climate model simulations. *J. Climate*, **26**, 6633–6648, https://doi.org/10.1175/JCLI-D-12-00813.1.

Huang, B., and Coauthors, 2017: Extended Reconstructed Sea Surface Temperature, version 5 (ERSSTv5): Upgrades, validations, and intercomparisons. *J. Climate*, **30**, 8179–8205, https://doi.org/10.1175/JCLI-D-16-0836.1.

Jenkins, A., P. Dutrieux, S. Jacobs, E. J. Steig, G. H. Gudmundsson, J. Smith, and K. J. Heywood, 2016: Decadal ocean forcing and Antarctic ice sheet response: Lessons from the Amundsen Sea. *Oceanography*, **29** (4), 106–117, https://doi.org/10.5670/oceanog.2016.103.

——, D. Shoosmith, P. Dutrieux, S. Jacobs, T. W. Kim, S. H. Lee, H. K. Ha, and S. Stammerjohn, 2018: West Antarctic Ice Sheet retreat in the Amundsen Sea driven by decadal oceanic variability. *Nat. Geosci.*, **11**, 733–738, https://doi.org/10.1038/s41561-018-0207-4.

Jin, D., and B. P. Kirtman, 2009: Why the Southern Hemisphere ENSO responses lead ENSO. *J. Geophys. Res.*, **114**, D23101, https://doi.org/10.1029/2009JD012657.

Jones, J. M., and M. Widmann, 2003: Instrument- and tree-ring-based estimates of the Antarctic oscillation. *J. Climate*, **16**, 3511–3524, https://doi.org/10.1175/1520-0442(2003)016<3511:IATEOT>2.0.CO;2.

——, and ——, 2004: Early peak in Antarctic oscillation index. *Nature*, **432**, 290–291, https://doi.org/10.1038/432290b.

——, R. L. Fogt, M. Widmann, G. J. Marshall, P. D. Jones, and M. Visbeck, 2009: Historical SAM variability. Part I: Century-length seasonal reconstructions. *J. Climate*, **22**, 5319–5345, https://doi.org/10.1175/2009JCLI2785.1.

Kidson, J. W., 1999: Principal modes of Southern Hemisphere low-frequency variability obtained from NCEP–NCAR reanalyses. *J. Climate*, **12**, 2808–2830, https://doi.org/10.1175/1520-0442(1999)012<2808:PMOSHL>2.0.CO;2.

Li, X., and Coauthors, 2021: Tropical teleconnection impacts on Antarctic climate changes. *Nat. Rev. Earth Environ.*, **2**, 680–698, https://doi.org/10.1038/s43017-021-00204-5.

Marshall, G. J., 2003: Trends in the Southern Annular Mode from observations and reanalyses. *J. Climate*, **16**, 4134–4143, https://doi.org/10.1175/1520-0442(2003)016<4134:TITSAM>2.0.CO;2.

Meehl, G. A., J. M. Arblaster, C. M. Bitz, C. T. Y. Chung, and H. Teng, 2016: Antarctic sea-ice expansion between 2000

and 2014 driven by tropical Pacific decadal climate variability. *Nat. Geosci.*, **9**, 590–595, https://doi.org/10.1038/ngeo2751.

Mo, K. C., and R. W. Higgins, 1998: The Pacific–South American modes and tropical convection during the Southern Hemisphere winter. *Mon. Wea. Rev.*, **126**, 1581–1596, https://doi.org/10.1175/1520-0493(1998)126<1581:TPSAMA>2.0.CO;2.

Naughten, K. A., P. R. Holland, and J. De Rydt, 2023: Unavoidable future increase in West Antarctic ice-shelf melting over the twenty-first century. *Nat. Climate Change*, **13**, 1222–1228, https://doi.org/10.1038/s41558-023-01818-x.

O'Connor, G. K., E. J. Steig, and G. J. Hakim, 2021: Strengthening Southern Hemisphere westerlies and Amundsen Sea low deepening over the 20th century revealed by proxy-data assimilation. *Geophys. Res. Lett.*, **48**, e2021GL095999, https://doi.org/10.1029/2021GL095999.

——, P. R. Holland, E. J. Steig, P. Dutrieux, and G. J. Hakim, 2023: Characteristics and rarity of the strong 1940s westerly wind event over the Amundsen Sea, West Antarctica. *Cryosphere*, **17**, 4399–4420, https://doi.org/10.5194/tc-17-4399-2023.

O'Reilly, C. H., J. Heatley, D. MacLeod, A. Weisheimer, T. N. Palmer, N. Schaller, and T. Woollings, 2017: Variability in seasonal forecast skill of Northern Hemisphere winters over the twentieth century. *Geophys. Res. Lett.*, **44**, 5729–5738, https://doi.org/10.1002/2017GL073736.

Paolo, F. S., L. Padman, H. A. Fricker, S. Adusumilli, S. Howard, and M. R. Siegfried, 2018: Response of Pacific-sector Antarctic ice shelves to the El Niño/Southern Oscillation. *Nat. Geosci.*, **11**, 121–126, https://doi.org/10.1038/s41561-017-0033-0.

Pritchard, H. D., S. R. M. Ligtenberg, H. A. Fricker, D. G. Vaughan, M. R. van den Broeke, and L. Padman, 2012: Antarctic ice-sheet loss driven by basal melting of ice shelves. *Nature*, **484**, 502–505, https://doi.org/10.1038/nature10968.

Rakthanmanon, T., B. Campana, A. Mueen, G. Batista, B. Westover, Q. Zhu, J. Zakaria, and E. Keogh, 2013: Addressing big data time series: Mining trillions of time series subsequences under dynamic time warping. *ACM Trans. Knowl. Discovery Data*, **7** (3), 1–31, https://doi.org/10.1145/2500489.

Raphael, M. N., and Coauthors, 2016: The Amundsen Sea low: Variability, change, and impact on Antarctic climate. *Bull. Amer. Meteor. Soc.*, **97**, 111–121, https://doi.org/10.1175/BAMS-D-14-00018.1.

Schneider, D. P., and E. J. Steig, 2008: Ice cores record significant 1940s Antarctic warmth related to tropical climate variability. *Proc. Natl. Acad. Sci. USA*, **105**, 12 154–12 158, https://doi.org/10.1073/pnas.0803627105.

——, and C. Deser, 2018: Tropically driven and externally forced patterns of Antarctic Sea ice change: Reconciling observed and modeled trends. *Climate Dyn.*, **50**, 4599–4618, https://doi.org/10.1007/s00382-017-3893-5.

——, and R. L. Fogt, 2018: Artifacts in century-length atmospheric and coupled reanalyses over Antarctica due to historical data availability. *Geophys. Res. Lett.*, **45**, 964–973, https://doi.org/10.1002/2017GL076226.

——, Y. Okumura, and C. Deser, 2012: Observed Antarctic interannual climate variability and tropical linkages. *J. Climate*, **25**, 4048–4066, https://doi.org/10.1175/JCLI-D-11-00273.1.

Scott Yiu, Y. Y., and A. C. Maycock, 2019: On the seasonality of the El Niño teleconnection to the Amundsen Sea region. *J. Climate*, **32**, 4829–4845, https://doi.org/10.1175/JCLI-D-18-0813.1.

Shepherd, A., and Coauthors, 2018: Mass balance of the Antarctic Ice Sheet from 1992 to 2017. *Nature*, **558**, 219–222, https://doi.org/10.1038/s41586-018-0179-y.

Silvano, A., and Coauthors, 2022: Baroclinic ocean response to climate forcing regulates decadal variability of ice-shelf melting in the Amundsen Sea. *Geophys. Res. Lett.*, **49**, e2022GL100646, https://doi.org/10.1029/2022GL100646.

Slivinski, L. C., and Coauthors, 2019: Towards a more reliable historical reanalysis: Improvements for version 3 of the Twentieth Century Reanalysis system. *Quart. J. Roy. Meteor. Soc.*, **145**, 2876–2908, https://doi.org/10.1002/qj.3598.

Smith, J. A., and Coauthors, 2017: Corrigendum: Sub-ice-shelf sediments record history of twentieth-century retreat of Pine Island Glacier. *Nature*, **549**, 292, https://doi.org/10.1038/nature23650.

Steig, E. J., Q. Ding, D. S. Battisti, and A. Jenkins, 2012: Tropical forcing of Circumpolar Deep Water Inflow and outlet glacier thinning in the Amundsen Sea Embayment, West Antarctica. *Ann. Glaciol.*, **53**, 19–28, https://doi.org/10.3189/2012AoG60A110.

——, and Coauthors, 2013: Recent climate and ice-sheet changes in West Antarctica compared with the past 2,000 years. *Nat. Geosci.*, **6**, 372–375, https://doi.org/10.1038/ngeo1778.

Trenberth, K. E., and L. Smith, 2005: The mass of the atmosphere: A constraint on global analyses. *J. Climate*, **18**, 864–875, https://doi.org/10.1175/JCLI-3299.1.

Turner, J., and Coauthors, 2004: The SCAR READER Project: Toward a high-quality database of mean Antarctic meteorological observations. *J. Climate*, **17**, 2890–2898, https://doi.org/10.1175/1520-0442(2004)017<2890:TSRPTA>2.0.CO;2.

——, T. Phillips, J. S. Hosking, G. J. Marshall, and A. Orr, 2013: The Amundsen Sea Low. *Int. J. Climatol.*, **33**, 1818–1829, https://doi.org/10.1002/joc.3558.

——, A. Orr, G. H. Gudmundsson, A. Jenkins, R. G. Bingham, C.-D. Hillenbrand, and T. J. Bracegirdle, 2017: Atmosphere-ocean-ice interactions in the Amundsen Sea Embayment, West Antarctica. *Rev. Geophys.*, **55**, 235–276, https://doi.org/10.1002/2016RG000532.

Valler, V., and Coauthors, 2024: ModE-RA: A global monthly paleo-reanalysis of the modern era 1421 to 2008. *Sci. Data*, **11**, 36, https://doi.org/10.1038/s41597-023-02733-8.

Weisheimer, A., N. Schaller, C. O'Reilly, D. A. MacLeod, and T. Palmer, 2017: Atmospheric seasonal forecasts of the twentieth century: Multi-decadal variability in predictive skill of the winter North Atlantic Oscillation (NAO) and their potential value for extreme event attribution. *Quart. J. Roy. Meteor. Soc.*, **143**, 917–926, https://doi.org/10.1002/qj.2976.

——, D. J. Befort, D. MacLeod, T. Palmer, C. O'Reilly, and K. Strømmen, 2020: Seasonal forecasts of the twentieth century. *Bull. Amer. Meteor. Soc.*, **101**, E1413–E1426, https://doi.org/10.1175/BAMS-D-19-0019.1.

Wilks, D. S., 2016: "The stippling shows statistically significant grid points": How research results are routinely overstated and overinterpreted, and what to do about it. *Bull. Amer. Meteor. Soc.*, **97**, 2263–2273, https://doi.org/10.1175/BAMS-D-15-00267.1.

Wright, M. J., A. Weisheimer, and T. Woollings, 2024: Multi-decadal skill variability in predicting the spatial patterns of ENSO events. *Geophys. Res. Lett.*, **51**, e2023GL107971, https://doi.org/10.1029/2023GL107971.